

xarov: a tool for neutrino flux generation from WIMPs

To cite this article: Qinrui Liu et al JCAP10(2020)043

View the <u>article online</u> for updates and enhancements.



IOP ebooks™

Bringing together innovative digital publishing with leading authors from the global scientific community.

Start exploring the collection-download the first chapter of every title for free.

χ aro ν : a tool for neutrino flux generation from WIMPs

Qinrui Liu,^a Jeffrey Lazar,^{a,b} Carlos A. Argüelles^b and Ali Kheirandish^{c,d}

^aDepartment of Physics & Wisconsin IceCube Particle Astrophysics Center, University of Wisconsin, Madison, WI 53706, U.S.A.

E-mail: qliu246@wisc.edu, jeffrey.lazar@icecube.wisc.edu, carguelles@fas.harvard.edu, kheirandish@psu.edu

Received August 14, 2020 Accepted September 8, 2020 Published October 16, 2020

Abstract. Indirect searches for signatures of corpuscular dark matter have been performed using all cosmic messengers: gamma rays, cosmic rays, and neutrinos. The search for dark matter from neutrinos is of particular importance since they are the only courier that can reach detectors from dark matter processes in dense environments, such as the core of the Sun or Earth, or from the edge of the observable Universe. In this work, we introduce $\chi aro \nu$, a software package that, in the spirit of its mythological Greek namesake $\chi \acute{\alpha} \rho \omega \nu$, bridges the dark sector and Standard Model by predicting neutrino fluxes from different celestial dark matter agglomerations. The flux at the point of production is either computed internally by $\chi aro \nu$ or is taken from user supplied tables. $\chi aro \nu$ then propagates this flux through vacuum or dense media and returns the expected neutrino yield at an observer's location. In developing $\chi aro \nu$, we have revisited and updated the production of neutrinos in dense media, updated the propagation of high-energy neutrinos, and studied the sources of uncertainty in neutrino transport. This package is coupled to a new calculation that includes electroweak corrections resulting in the most up-to-date and complete repository of neutrino fluxes from dark matter decay and annihilation over the energy range of 1 GeV to 10 PeV coming from the Earth, the Sun, and the Galactic halo.

Keywords: dark matter simulations, neutrino astronomy, neutrino detectors

ArXiv ePrint: 2007.15010

^bDepartment of Physics & Laboratory for Particle Physics and Cosmology, Harvard University, Cambridge, MA 02138, U.S.A.

 $[^]c{\rm Department}$ of Physics, The Pennsylvania State University, University Park, PA 16802, U.S.A.

^dCenter for Multimessenger Astrophysics, Institute for Gravitation & the Cosmos, The Pennsylvania State University, University Park, PA 16802, U.S.A.

1	Introduction	1
2	Indirect detection of dark matter	3
3	Neutrino yields from annihilation and decay: algorithm description	5
4	Neutrino transport with $ u$ SQuIDS	9
	4.1 Galactic flux propagation	11
	4.2 Solar flux propagation	11
	4.3 Earth flux propagation	12
5	Secluded dark matter	12
6	Comparison to other calculations and sources of uncertainty	15
	6.1 Comparison to other calculations	15
	6.2 Effects of the neutrino oscillation parameters	16
	6.3 Effects of the neutrino cross section	17
7	Conclusion	19

1 Introduction

Contents

The Standard Model (SM) of particle physics — a theory with exceptional predictive power and confirmed by a plethora of measurements [1] — has failed to predict the existence of non-zero neutrino masses and provide a viable dark matter (DM) candidate. In the search for beyond Standard Model Physics, neutrinos, DM, and the Sun are intimately connected.

Though the observation of non-zero neutrino masses has been confirmed using both anthropogenic and natural sources [2], the first sign of neutrino flavor conversion was hinted by the mismatch between solar neutrino flux calculations [3, 4] and data [5]; see [6, 7] for historical summary and review. Neutrinos, which interact only via the weak force, are the only cosmic messengers that can escape dense environments, such as the center of the Sun, unimpeded. They yield information about their place of origin [8] and their behaviour in extreme environments [9]. The existence of DM has been established by astrophysical and cosmological observations [10-14]. In the standard Λ CDM model of cosmology, DM comprises about 85% of the Universe's present matter content [15]; however, the nature and identity of DM are not currently known. A number of DM candidates have been put forward, including massive compact halo objects (MACHOs), weakly interacting massive particles (WIMPs), axions, and sterile neutrinos. Among these candidates, WIMPs are a class of elementary particles beyond the Standard Model which were thermally produced in the early Universe. WIMPs are neutral and assumed to be stable over cosmological scales. They interact gravitationally, and are assumed to possess additional interactions at or below the weak scale; in fact, DM-neutrino interactions often appear in neutrino mass generation models [16–24]. These so-called *scotogenic* mass generation models have been proposed using sub-eV DM [25], dark sectors below the electroweak scale [22, 26], and heavy DM [27, 28].

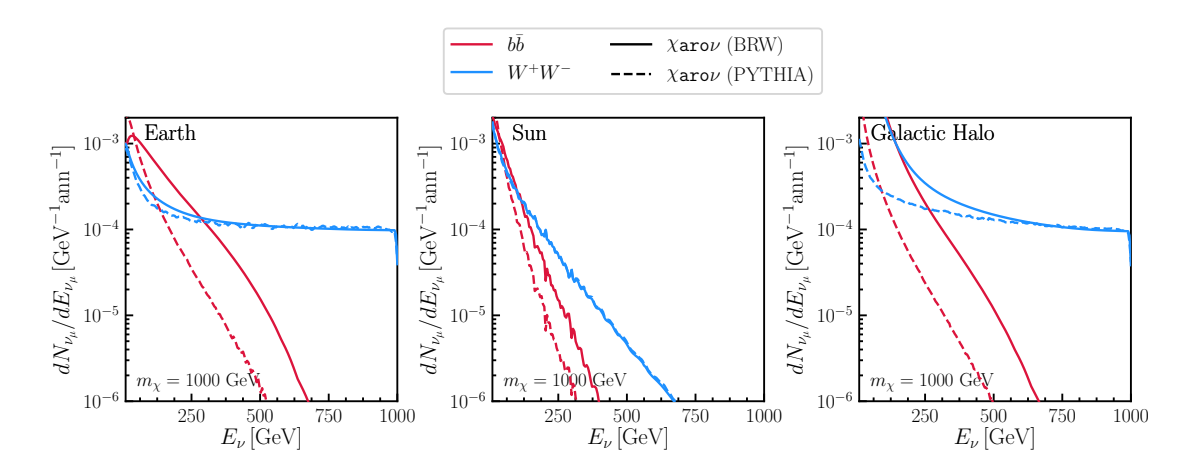


Figure 1. χ arov's predicted ν_{μ} yield at Earth's surface for DM annihilation in the Earth, Sun, and the Galactic Halo. In this work we use the primary flux obtained from the recent BRW calculation [109], which includes polarization of annihilation and decay products as well as a consistent treatment of the EW correction as our nominal flux. The dotted lines show our results using the primary flux from PYTHIA, which has a limited implementation of the EW correction. We show results for the normal mass ordering.

WIMP DM can accumulate in the center of dense celestial bodies, such as the Sun, and annihilate into SM particles [29–33]. In the standard scenario, these particles can annihilate or decay to SM particles, yielding high-energy neutrinos that, unlike other products, can escape the Sun. The detection of these neutrinos would provide a smoking-gun signature of DM since the only other source of high-energy solar neutrinos are those produced in cosmic-ray interactions in the solar corona, which have a small and well-predicted flux [34–39], yet to be measured [40]. By looking for excesses of neutrinos coming from the direction of the Sun [41–102], neutrino observatories such as ANTARES, Baikal, Baksan, IceCube, and Super-Kamiokande, have set upper limits on the WIMP-nucleon scattering cross section [103–108]. In the future, more stringent constraints can be set by Hyper-Kamiokande, Baikal-GVD, Km3Net, and, IceCube-Gen2 as they are expected to have improved sensitivities.

Beyond the Sun, indirect searches look for evidence of WIMP annihilation or decay to SM particles in other regions that are expected to have large DM content, such as the Galactic center and Earth's core [110, 111]. Intensive efforts have also been made to detect such signatures from these objects, but so far only constraints have been placed by looking at the Earth [112, 113] and the Milky Way [114–119]; see [120] for a recent review. Earth and Solar WIMP searches are complementary to direct detection strategies. In the case of direct detection, one looks for energy deposited in a calorimeter by WIMPs scattering off nuclei. The detection medium for these searches can be liquid noble gases such as argon or xenon [121–123], which provides the strongest constraint on the spin-independent WIMP-nucleon cross section; or an organic compound [124], which is more sensitive to the spin-dependent WIMP-nucleon cross section. This difference arises from the fact that axial-vector WIMP coupling to a nucleus is enhanced by having unpaired protons or neutrons [125].

In this work, we introduce a new tool, $\chi \text{aro} \nu$ [126], to compute the neutrino fluxes from WIMP annihilations and decays in the Sun, the Earth, and the Galactic Halo. For DM masses below the electroweak (EW) scale, the neutrino flux produced from DM annihilation

¹Pronounced "Charon".

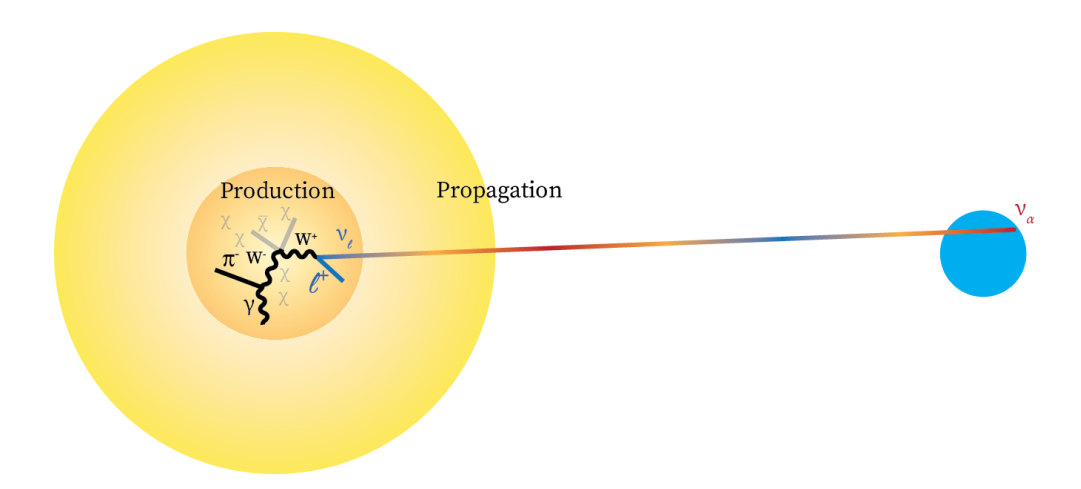


Figure 2. Diagram depicting an example of WIMP annihilation to SM particles. These primary annihilation products, which in this illustration is a W^+W^- pair, decay to other SM particles of which only neutrinos are able to leave the production region. The neutrino is indicated as a color-oscillating line to signify neutrino flavor change.

or decay is computed using PYTHIA-8.2, while for masses above this scale a recent calculation by Bauer, Rodd, and Webber (BRW) $[109]^2$ is used. The propagation of neutrinos from their production region to the detector is computed with the help of the neutrino propagation software ν SQuIDS [127, 128]. Our resulting fluxes below the EW scale are in good agreement with the WimpSim [58] calculation, while above it we provide comparisons of our calculation with the existing calculations WimpSim and the Poor Particle Physicist Cookbook (PPPC) [84, 129]. Furthermore, we quantify the uncertainties in the transport of neutrinos that arises from neutrino cross sections and neutrino oscillation parameters. For completeness, our package additionally contains a calculation of the WIMP capture rate in the Sun and Earth and a computation of the J-factor to be used for the Galactic contribution. Additionally, our code also supports the secluded DM scenario [130], where DM annihilates to an unstable long-lived mediator which in turn decays to SM particles. Figure 1, shows our new calculation for the flux of DM annihilation in the Sun, Earth, and Galactic Halo with our estimated uncertainties due to neutrino transport.

The rest of this article is organized as follows: in section 2, we describe the theoretical background relevant for indirect DM searches. In section 3, we explain our procedure for generating neutrinos at the production site. Section 4 describes the procedure for propagating these fluxes from their birthplace to the detector. In section 5, we discuss the case in which there is a long-lived mediator that connects the dark sector to the SM. Section 6, compares our results with current widely used calculations WimpSim [58] and PPPC [84, 131] as well as quantifies the total uncertainty associated with signal generation in neutrino indirect detection searches. Finally, in section 7 we conclude.

2 Indirect detection of dark matter

If DM is allowed to annihilate or decay to SM particles, experiments can detect these primary products of annihilation or decay or their secondaries as a signature of DM. These attempts to find DM through such products are known as indirect detection searches. In order to carry

²The results of this calculation are publicly available at https://github.com/nickrodd/HDMSpectra.

out these searches, one must know both where one expects large quantities of DM and the spectral shape of the signal. In this section, we briefly discuss the production of neutrinos from these regions.

After an overdensity of DM has formed, DM can produce detectable signatures either via annihilation or decay to SM particles. The spectral shape of the expected signal distribution depends on the primary channel, as well as any propagation effects, while the overall normalization is set by the rate of annihilation or decay. Signals coming from the Galactic Halo are usually parametrized by the so-called *J*-factor, given by:

$$J_{\theta} = \begin{cases} \int_{\Delta\Omega} \int_{\text{l.o.s.}} \rho^{2}(\theta, l) dl \, d\Omega & \text{(annihilation),} \\ \int_{\Delta\Omega} \int_{\text{l.o.s.}} \rho(\theta, l) dl \, d\Omega & \text{(decay),} \end{cases}$$
 (2.1)

where ρ is the DM density profile, θ is the direction in the sky in a right-handed coordinate system centered at the Earth with one of its axes aligned with the direction to the Galactic Center (GC), and the integral is along the line-of-sight (l.o.s.). The l.o.s is related to the direction given by θ and the distance from the GC to the point of annihilation or decay, r, by $r^2 = r_{\odot}^2 + l^2 - 2lr_{\odot}\cos\theta$, where l is the distance along the l.o.s.

After obtaining the J-factor, one can then compute the expected distribution of neutrinos from a given direction at the detector as

$$\Phi_{\nu,\text{det}} = \frac{1}{4\pi} \frac{dN_{\nu}}{dE_{\nu}} J_{\theta} \times \begin{cases} \frac{\langle \sigma_{A} v \rangle}{\kappa m_{\chi}^{2}} & \text{(annihilation)}, \\ \frac{\Gamma_{\chi}}{m_{\chi}} & \text{(decay)}, \end{cases}$$
 (2.2)

where dN_{ν}/dE_{ν} is the number of signal events per unit energy per annihilation or decay at the detector which differs from the flux at production by oscillation effects and energy redshift; Γ_{χ} is the rate at which the DM decays per DM particle; $\langle \sigma_A v \rangle$ is the DM annihilation cross section averaged over the DM velocity distribution; and κ is 2 for Majorana DM and 4 Dirac DM. The DM velocity distribution is assumed to be a Maxwellian distribution in the Standard Halo Model, which is favored by recent simulations [132], though non-thermal components could be present due to accretion. This averaging is necessary since in general the annihilation cross section is velocity-dependent, but its functional form is not known. In fact, the above expression is only accurate for velocity-independent dark matter interactions, since, in general, the velocity distribution is location dependent and cannot be factorized as in eq. (2.2). For generalization of the treatment above see [133–135] for *J*-factor independent implementations, for treatments of *p*-wave annihilation [136, 137], for Sommerfeld-enhanced cross section [138–141], for generalized *J* factors [142, 143], and for a recent compendium and uncertainty estimation [144]. Thus, for a given DM mass, and annihilation or decay channel searches looking at the GH are sensitive to the parameters $\langle \sigma_A v \rangle$ or Γ_{χ} , respectively.

Searches looking for DM signatures coming from the center of the Sun or Earth, on the other hand, are sensitive to the DM-nucleon scattering cross section. To understand why this is, it is useful to examine the differential equation governing the number of DM particles in a source, given by

$$\frac{dN}{dt} = \begin{cases}
C - AN^2 - EN & \text{(annihilation),} \\
C - DN - EN & \text{(decay).}
\end{cases}$$
(2.3)

Here, the C is the rate of WIMP accretion due to capture, A is the thermally-averaged WIMP annihilation cross section per unit volume, and D and E are respectively the decay and evaporation rates per DM particle [33, 125]. For DM with masses above a few GeV, the rate of evaporation is expected to be negligible [33, 145]. Thus these equations are solved by

$$N(t) = \begin{cases} \sqrt{\frac{C}{A}} \tanh(\sqrt{CA}t) & \text{(annihilation)}, \\ e^{-Dt} + \frac{C}{D} & \text{(decay)}. \end{cases}$$
 (2.4)

Whether or not the DM ensemble is in equilibrium depends on the capture and annihilation or decay rate; however, the DM ensemble is expected to be in equilibrium in the Sun [146]. In the case of the Earth, on the other hand, this equilibrium condition is not expected to be satisfied [147]. When in equilibrium, i.e. in the Sun, we can set the left hand side of eq. (2.3) to zero, giving that the capture rate is given by

$$C = \begin{cases} AN^2 & \text{(annihilation)}, \\ DN & \text{(decay)}. \end{cases}$$
 (2.5)

This implies that the quantities experiments are sensitive to, i.e. the annihilation and decay rates, are directly proportional to the capture rate at equilibrium. By default, $\chi \text{aro} \nu$ calculates the capture rate originally given in [148] with an up-to-date solar model [149], but these can be changed by the user, using for example [125, 150–152]. When interactions are rare, the capture rate is linearly proportional to the DM-nucleon scattering cross section, $\sigma_{\chi N}$, which enables direct comparison to direct searches, which also probe $\sigma_{\chi N}$. These two approaches though are complementary since they depend on different parts of the DM velocity distribution; the capture rate in the Sun is increased when DM is slower [153], while the direct detection scattering rate has the opposite effect. This complementarity has been recently exploited to obtain velocity-independent constraints by combining results from the IceCube and PICO experiments [154].

From these sources, the expected flux at the detector can be expressed as

$$\Phi_{\nu, \text{det}} = \frac{\Pi_x}{4\pi d^2} \frac{dN_\nu}{dE_\nu},\tag{2.6}$$

where T_x is the total rate of annihilation, $T_{\rm ann}$, or decay, T_{χ} , from the source; and d is the mean distance from the detector to the source. The symbol $T_{\rm dec}$ should not be confused with the symbol $T_{\rm dec}$, which is the rate of decay per DM particle.

To compute the neutrino flux that is expected at a detector, the next steps are the computation of neutrino yield at the source and the propagation of those neutrinos from the source to the detector. A graphic illustrating these processes is shown in figure 2.

3 Neutrino yields from annihilation and decay: algorithm description

We will now turn our discussion to the case of simulating the neutrino yield from DM annihilation and decay. Here, we utilize a Monte Carlo approach to compute neutrino flux at production and integro-differential equation to propagate the neutrinos. A high-level diagram of this process is shown in figure 3 and the result of the algorithm is shown in figure 4 for DM masses below and above the EW scale.

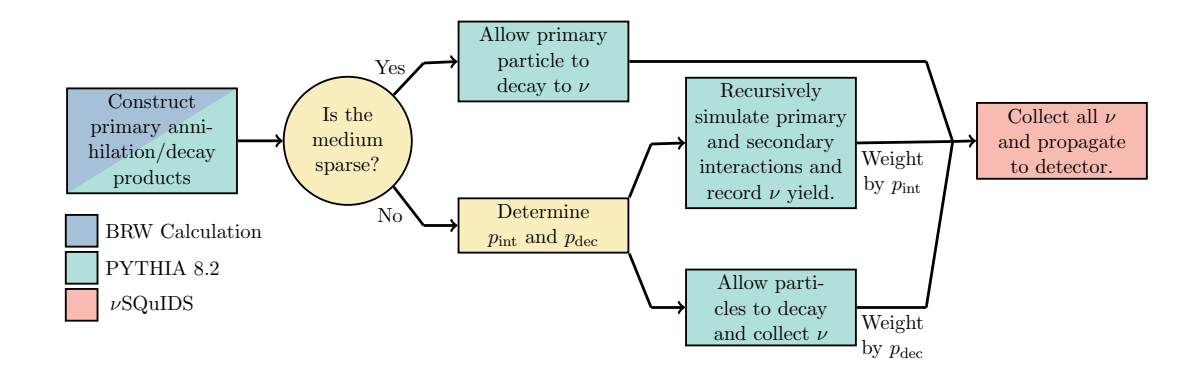


Figure 3. Diagram of code structure. Flow chart depicting the major steps in the calculating flux from DM annihilation or decay. The light yellow boxes indicate direct calculation or decision making; other colors indicate the main program used in each step.

In our simulation, we assume that the parent DM particles are at rest. This means that in the case of annihilation, each particle of the primary pair carries energy equal to the mass of the DM particle, m_{χ} , and in the case of decay, each particle carries energy equal to $m_{\chi}/2$. In both scenarios, the momenta of the primary pair are anti-aligned. Therefore, the computation for both scenarios are identical up to the mass. Therefore for conciseness, we will only focus on annihilation in the following discussion.

Since the interaction of DM with the SM is unknown, we take the pragmatic approach of computing the neutrino spectra for DM annihilation to $q\bar{q}$, gg, W^+W^- , Z^0Z^0 , HH, l^+l^- , and direct neutrino channels $\nu_{\alpha}\bar{\nu}_{\alpha}$; the latter channel is relevant in the case of Kaluza-Klein DM [50]. Here, $q\bar{q}$ are the six quarks, l^+l^- are the three charged leptons, and $\nu_{\alpha}\bar{\nu}_{\alpha}$ are the three neutrino flavors. The neutrino yield depends on the interplay of two variables: the primary particles produced and the environment in which production takes place. In sparse environments, those where the interaction lengths of particles are much longer than decay lengths, neutrinos can be formed as the primary decay or annihilation products, or as secondary products produced after the primary particle hadronizes and showers. In dense environments, on the other hand, this condition is not satisfied; the competition between interactions of the produced particles with matter and their decay process modifies the final neutrino spectrum. Therefore, one must compute the secondary particles' interaction lengths in order to precisely predict the neutrino fluxes.

In this work, we compute the fluxes at production using Pythia 8.2 with some modifications, since a vacuum environment is assumed by default in Pythia. For WIMP masses above $500\,\mathrm{GeV}$, we use the BRW calculation of the initial flux.

After accounting for hadronization and final states radiation of the primary particles, we simulate the interaction of the products with their environment. This involves determining whether or not the environment is sparse as previously defined, which in general depends on the particle. For all particles considered in this paper, the Galactic Halo is a sparse environment, and as such all particles produced there are allowed to decay without interacting. In the case of the core of the Sun or Earth, an evaluation of particle interactions is needed. Here, we discuss energy losses of hadrons, created from hadronization of quarks, and charged leptons in matter. In the following text, we will enumerate our treatment of particle interactions by cases.

Hadrons: except the top quark, which will immediately decay, all quarks will promptly hadronize. The resulting hadrons will interact with the matter in the production environment. The mean interaction time, τ_{int} , for a given hadron is given by

$$\tau_{\rm int} = (n\sigma v)^{-1} \approx 5.5 \times 10^{-8} \ s \times \left(\frac{\rm g/cm^3}{\rho}\right) \left(\frac{\rm mb}{\sigma}\right) \beta^{-1},$$
 (3.1)

where ρ is the density of the medium, σ is the hadron-nucleon scattering cross section, and β is the velocity of the hadron in natural units.

When the lifetime of the hadron is very short compared to the mean interaction time, the hadron is allowed to decay freely since energy losses due to interactions will be negligible. When the interaction and decay times are comparable, which is the case of hadrons that contain bottom (b) or charm (c) valence quarks, we weight our simulation according to the rate of these two processes. To carry out this weighting, we assume that hadrons containing b or c quarks have a similar hadron-nucleon cross sections, which are approximately, $\sigma_{b/c-\rm meson} \sim 14$ mb for mesons and $\sigma_{b/c-\rm baryon} \sim 24$ mb for baryons [155].

When a hadron containing b or c valence quarks is created in the simulation, we assume there is a probability of interacting and a probability of decaying given by

$$p_{\rm int} = \frac{\gamma \tau_{\rm dec}}{\tau_{\rm int} + \gamma \tau_{\rm dec}} \text{ and } p_{\rm dec} = \frac{\tau_{\rm int}}{\tau_{\rm int} + \gamma \tau_{\rm dec}},$$
 (3.2)

respectively, where $\tau_{\rm dec}$ is the rest-frame lifetime of the hadron and $\tau_{\rm int}$ is the mean time between interactions. Both interaction and decay are then simulated. In the case of decay, all products are weighted by $p_{\rm dec}$. In the case of interaction, one the other hand, the hadron is given a new energy E' and weighted by $p_{\rm int}$, and this process is recursively carried out until the hadron has lost all kinetic energy. In this procedure, low-energy neutrinos produced in hadronic showers initiated by the aforementioned hadron are not tracked, and thus we underestimate the low-energy flux; see [100] for a detailed low-energy calculation. In this work, we set $E' = \langle Z_x \rangle E_0$ where is $\langle Z_x \rangle$ is the average fractional energy transfer, and E_0 is the energy of the hadron before interaction. We follow the estimates of [156] and set $\langle Z_b \rangle = 0.7$ and $\langle Z_c \rangle = 0.6 \frac{m_c}{m_{\rm hadron}}$. $\chi_{\rm aro}\nu$ and WimpSim use this energy loss estimation method, while PPPC samples from an energy loss distribution; we have checked that these two approaches yield comparable results.

Using eq. (3.1) to estimate the ratio of $\gamma \tau_{\rm dec}$ to $\tau_{\rm int}$ for hadrons composed only of up, down, and strange quarks gives a number of order 10^4 and 10^3 in the Sun and Earth respectively for $m_{\chi}=1$ GeV. These ratios grow to 10^8 and 10^7 for $m_{\chi}=1$ TeV. Thus, one can safely assume that such hadrons, namely π^{\pm} , K^{\pm} , K^{0}_{L} , and neutrons are fully stopped on account of rapid interactions before decaying.

Charged leptons: the rate at which charged leptons lose energy in a plasma, such as the center of the Sun, is given in [157]. We find that the rate of energy loss, $\frac{dE}{dt}$, is larger than 10^9 GeV/s. This gives that the stopping time is bounded by $\tau_{\text{stop}} = m_{\chi}/(dE/dt)$. Computing the ratio of τ_{stop} to $\gamma \tau_{\text{dec}}$ for tauons (τ) and muons (μ) leads to the conclusion that in the relevant energies, the τ will promptly decay, but most μ will stop before decaying.

In the Earth, charged leptons lose energy through ionization, bremsstrahlung, photonuclear interaction, and electron pair production, which we estimate using the Bethe-Bloch formula [1]. The interaction length of τ in Earth is significantly larger than the decay length up to τ energies of 10⁹ GeV [158]. Thus for the DM mass range under discussion in this work, one can assume the τ decays at production without interacting. Muons are longer lived, and at μ energies above a few GeV the interaction length is much shorter than the decay length. As in the case of the Sun, they can be assumed to come to rest before decaying.

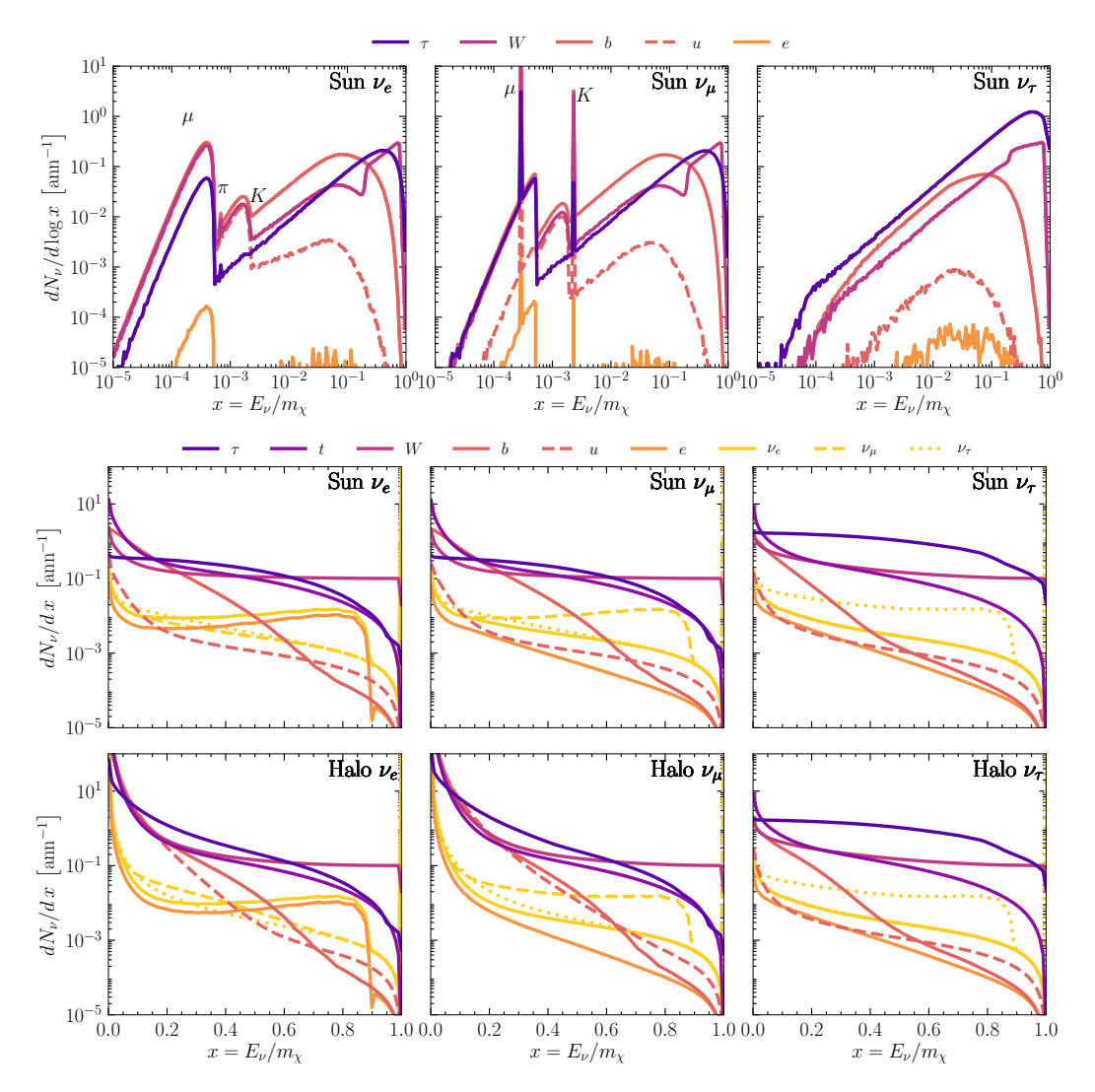


Figure 4. Differential neutrino flux at production. We show spectra for several representative annihilation channels, indicated by different line colors. The top panel shows the spectra for $m_\chi=100\,\mathrm{GeV}$ in the center of the Sun, generated without EW correction and with decays from stopped particles. Features related to μ , π , and K decays are indicated by their respective symbols. The two-row linear scale panel at the bottom shows spectra for a DM mass of $m_\chi=1000\,\mathrm{GeV}$ with EW correction and without decays from stopped particles. Different polarization states are averaged over. Due to EW corrections, direct neutrino channels no longer show a two-body decay distribution, but have a low-energy tail. The top row corresponds to the center of the Sun, while the bottom row is for the Galactic Halo. The different columns indicate the neutrino flavor, from left to right: electron, muon, and tau flavored neutrinos. For DM decay, m_χ should be multiplied by a factor of 2 and x be replaced by $x=2E_\nu/m_\chi$. Quarks not shown in this plot lie between the dashed and solid u and b lines, and differ only by a normalization.

Long-lived particles: long-lived hadrons, π^{\pm} , K^{\pm} , K_L^0 , and neutrons, are either fully absorbed by matter or decay after being stopped. Among them, π^- and K^- are captured by matter and would form atom-like systems, which prohibits them from further decays [159]. Due to different interactions of K^0 and \bar{K}^0 with nucleons, which causes quantum coherence loss, K_S^0 are regenerated from K_L^0 continuously and followed by hadronic decays [160].

Stopped μ^{\pm} , π^{+} , and K^{+} continue to decay at rest. Neutrinos from decay of stopped particles are produced at energies below 1 GeV, thus are not of great importance for current indirect searches. $\chi_{aro\nu}$ provides an option to compute these low-energy neutrinos using PYTHIA. These neutrinos have also been considered in previous calculations, e.g. they are included in PPPC using Geant4 [84], a technique first developed in [100]; see also [99, 101, 102].

Polarizations and EW corrections: for DM masses above the EW scale, the neutrino flux generation in $\chi_{aro\nu}$ is coupled to a new computation of the EW correction which also accounts for polarization of annihilation and decay states and the evolution of the polarized particles to the EW scale [109]. As EW interactions are not fully implemented in PYTHIA, this calculation incorporates a more complete consideration such as the missing triple gauge couplings in the EW sector. Polarization and EW correction effects are also implemented in PPPC, which takes a different approach by augmenting leading order EW correction term [129]. Other works have studied the effects of polarization of annihilation or decay products without EW correction in [161, 162]. We find that the inclusion of this new estimation of EW corrections and polarization gives rise to different spectra, which may be softer or harder depending on the channel and DM mass.

4 Neutrino transport with ν SQuIDS

As in section 3, we discuss two cases of interest: neutrino-opaque and neutrino-transparent media. To distinguish between these scenarios, we define a neutrino-opaque environment as those where the neutrino interaction length is less than the distance the neutrino needs to travel to exit the source and neutrino-transparent environments otherwise. The neutrino interaction length is an energy dependent quantity given by

$$\lambda^{\text{int}}(E_{\nu}) = \left[n_N \sigma^{\text{tot}}(E_{\nu}) \right]^{-1} = \left[n_N \sigma^{\text{CC}}(E_{\nu}) + n_N \sigma^{\text{NC}}(E_{\nu}) \right]^{-1}, \tag{4.1}$$

where n_N is the number density of nucleons, $\sigma^{\rm CC}$ is the neutrino-nucleon charged-current cross section, and $\sigma^{\rm NC}$ the neutral-current cross section; the neutrino-electron cross section is a subdominant contribution to the interaction rate and can be neglected in most applications [163]. These latter terms define, respectively, the charged- and neutral-current interaction lengths [163].

For electron and muon neutrinos with energies above $100\,\mathrm{GeV}$ [164], the interaction length is essentially identical, and thus the interaction rate will be the same for both flavors of neutrinos. On the other hand, the ν_{τ} charged-current cross section differs significantly from the ν_{e} and ν_{μ} charged-current cross sections due to phase-space suppression, which results in a 30% difference at $100\,\mathrm{GeV}$ [165–167]; see [168] for a discussion of this in neutrino oscillation experiments. This means that below this energy, environments will be less opaque to tau neutrinos than to neutrinos of other flavors. Furthermore, the neutrino yield is flavor-dependent because the competition between interaction and decay differs for each flavor of charged lepton. We do not consider neutrinos from electrons since they do not decay, and, in this work, we do not include neutrinos produced by showers induced by electrons. Muons can decay, but since they are relatively long-lived, they will interact with a medium as discussed in section 3, losing energy and reducing the yield of high-energy neutrinos. Tauons, on the other hand, are short-lived, and will decay quickly enough to give a significant fraction of their energy to the produced neutrino in a process known as tau-neutrino regeneration [169].

To be concrete, for energies less than 10 PeV and densities of $\mathcal{O}(g/cm^3)$, the tauon will decay promptly to a hard neutrino.

After accounting for the flavor dependence of secondary neutrino yield due to both the yield of neutrinos per charged-current interaction and the interaction rate itself, one must consider the effect of neutrino flavor change, commonly called neutrino oscillations [170]. This phenomena is due to the fact that the mass and flavor bases are misaligned. These two bases are related by a unitary transformation known as the Pontecorvo-Maki-Nakagawa-Sakata (PMNS) or neutral-lepton-mixing matrix, U. This three-by-three, complex-valued matrix can be parameterized as a product of two real and one complex rotations, namely $U = R_{23}\bar{R}_{13}R_{12}$ [1] where R_{ij} is a real rotation and \bar{R}_{13} a complex rotation. The real angles involved in this parameterization have been measured to percentage levels [2] and there is hint of a non-zero complex phase [171]. The elements of this matrix, which relate the flavor and mass states, dictate the flavor transition amplitude, while the characteristic length over which transitions occur depends on the mass-squared differences between the mass eigenvalues. This oscillation length is given by

$$\lambda^{\text{osc,i}} = 4\pi \frac{E_{\nu}}{\Delta m_{i1}^2},\tag{4.2}$$

where Δm_{i1}^2 , with i=2 or 3, are the two neutrino mass-squared-differences which have been measured from terrestrial and solar neutrino experiments and are known to the few-percent level [2].

In this work, we use the ν SQuIDS [127, 128] software package to consistently account for the above effects in neutrino transport. This package represents the initial flavor in the density matrix formalism, $\rho_{\alpha} = |\nu_{\alpha}\rangle \langle \nu_{\alpha}|$, the evolution of which is governed by

$$\frac{\partial \rho}{\partial r} = -i \left[H, \rho \right] - \left\{ \Gamma, \rho_i \right\} + \int_E^\infty F(\rho, \bar{\rho}, r, E', E) dE', \tag{4.3}$$

where H is the full neutrino Hamiltonian, including both the neutrino kinetic terms and matter potentials; Γ is the interaction rate; and F is a functional which encodes the cascading down of neutrinos due to charged and neutral current processes, see [128] for details. The terms in this equation depend on the environment traversed by the neutrino, as well as the PMNS matrix and neutrino cross sections. For our nominal results and plots shown in this work we set the oscillation parameters to the best-fit values for normal ordering from NuFit-4.1 [2, 172] and model the neutrino nucleon cross section using the nuSIGMA software package [173].

After the neutrinos exit their production region — in this work the Sun center, the Earth center or the Galactic Halo —they must be propagated to the detector location at Earth. In this voyage, we need to account for neutrino oscillations in vacuum and propagation inside Earth if the flux traverses significant matter, which imply that the spectrum for ν_{α} at the detector can be written as

$$\frac{dN_{\nu_{\alpha}}^{\oplus}}{d\Omega dE_{\nu_{\alpha}}dt} = f(\Omega) \sum_{\beta}^{3} \frac{dN_{\nu_{\beta}}^{\text{prod}}}{dE_{\nu_{\beta}}} \bar{P}_{\nu_{\beta} \to \nu_{\alpha}}(d, E_{\nu}), \tag{4.4}$$

where $dN_{\nu_{\beta}}^{\text{prod}}/dE_{\nu_{\beta}}$ is the neutrino yield per annihilation or decay computed in section 3; $\bar{P}_{\nu_{\beta}\to\nu_{\alpha}}(d,E_{\nu})$ is the production-region-averaged probability of ν_{β} oscillating to ν_{α} at distance

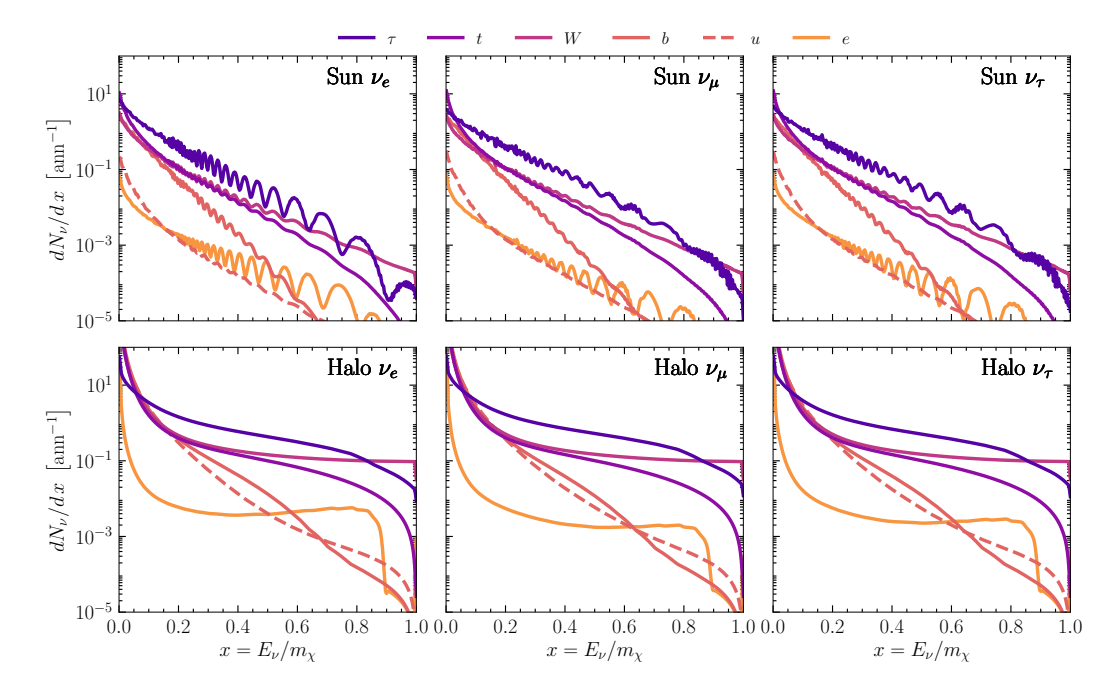


Figure 5. Neutrino flux from DM annihilation at Earth's surface. Colors and line styles have the same meaning as in figure 4. Results in the top panel are computed with a zenith angle of 60° while those in the bottom panel are computed with a zenith angle of 180°. The DM mass have been set to 1 TeV for annihilation; for decay it should be read as 2 TeV and x should be replaced by $x = 2E_{\nu}/m_{\chi}$.

d with energy E_{ν} ; and $f(\Omega)$ is a function which encodes information about the rate of neutrino production and the geometry of the source. The rate T is process- and location-dependent and the specifics of this dependence are discussed in section 2.

In what follows, we give additional details relevant for the propagation in the three production environments considered in this work. The result of these processes is summarized in figure 5.

4.1 Galactic flux propagation

The distance between the Galactic Center and the Earth is sufficiently large that all currentand next-generation detectors do not have sufficient energy resolution to resolve individual oscillations. Thus, the energy and distance dependence in eq. (4.4) is given by its average value. In this regime, the flavor transition probabilities are given by

$$P(\nu_{\alpha} \to \nu_{\beta}) = \sum_{i}^{3} |U_{\alpha i}|^{2} |U_{\beta i}|^{2} \approx \begin{bmatrix} 0.55 & 0.18 & 0.27 \\ 0.18 & 0.44 & 0.38 \\ 0.27 & 0.38 & 0.35 \end{bmatrix}, \tag{4.5}$$

where parameters are obtained by using the best-fit values from NuFit-4.1 with normal ordering.

4.2 Solar flux propagation

Neutrinos produced in the solar center must travel through solar matter, vacuum, Earth's atmosphere, and the Earth itself to get the detector. In this article, we use the standard solar model given in [149] to propagate neutrinos from center of the Sun to the surface of the

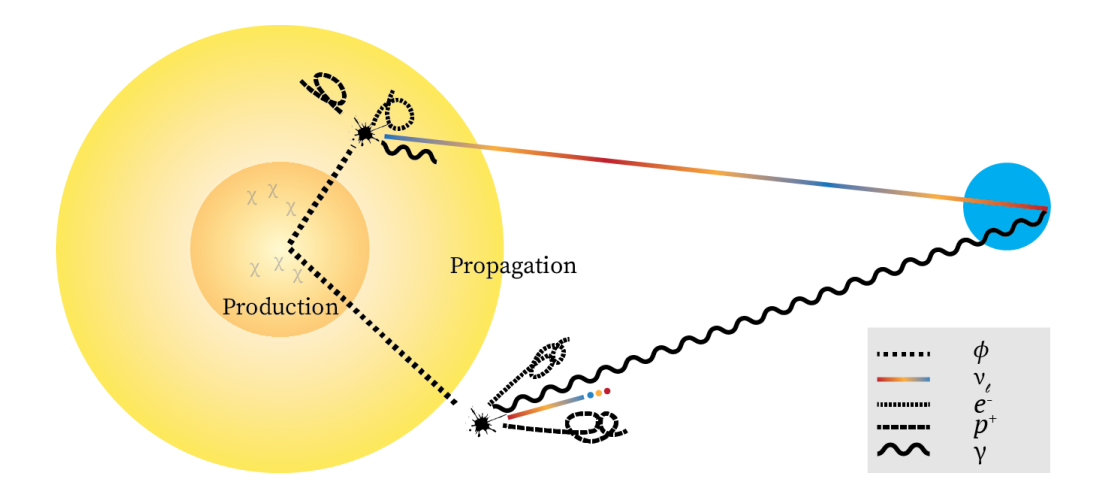


Figure 6. Illustration of the secluded DM scenario. In this scenario the DM is secluded from the SM and predominantly communicates with it via a long-lived annihilation or decay mediator, ϕ . The dotted line represents this mediator. If the average decay length is less than the radius of the source, then as in the standard case, only neutrinos will escape. On the other hand, if this length is longer than the radius of the source, then neutrinos, γ -rays, e^+e^- and $p\bar{p}$ can escape the source.

Sun. ν SQuIDS accounts for matter effects in solar matter in this process. Assuming the DM is at rest relative to the Sun, the neutrino flux will be emitted isotropically from the center of the Sun.

To compute the expected flux at the detector, one must consider both the detector position and the Earth's position relative to the Sun. We can compute the time-dependent flux which changes with the solar zenith angle, as well as the time-integrated flux which depends on the time window.

4.3 Earth flux propagation

For DM clustered in the center of the Earth, neutrinos propagate from the Earth center to the detector. The Earth density and composition is parameterized by the Preliminary Reference Earth Model (PREM) [174]. Since the detector is in Earth, there is no time-dependent information of the flux; namely we assume that there is no relative motion between the DM distribution and the detector. As discussed above, we can use ν SQuIDS to propagate neutrinos from the center of the Earth to the location we are interested in.

5 Secluded dark matter

Now we turn our focus to an alternative scenario in which DM particles are assumed to be *secluded* from the SM [130]. Secluded DM interacts with the SM through a dark-sector mediator while direct couplings to the SM are greatly suppressed.

In this model, DM annihilates to a pair of long-lived mediators, ϕ , which then decay to SM particles; these SM particles will then decay to stable messenger particles as discussed previously. A graphic illustrating the secluded DM scenario is shown in figure 6. Signatures of secluded DM from the Sun or Earth have been studied in [69, 175–179]. This model includes two additional parameters besides m_{χ} : m_{ϕ} and λ_{ϕ} , the mass and decay length of the mediator. The introduction of these new parameters affects the flux calculation in a number

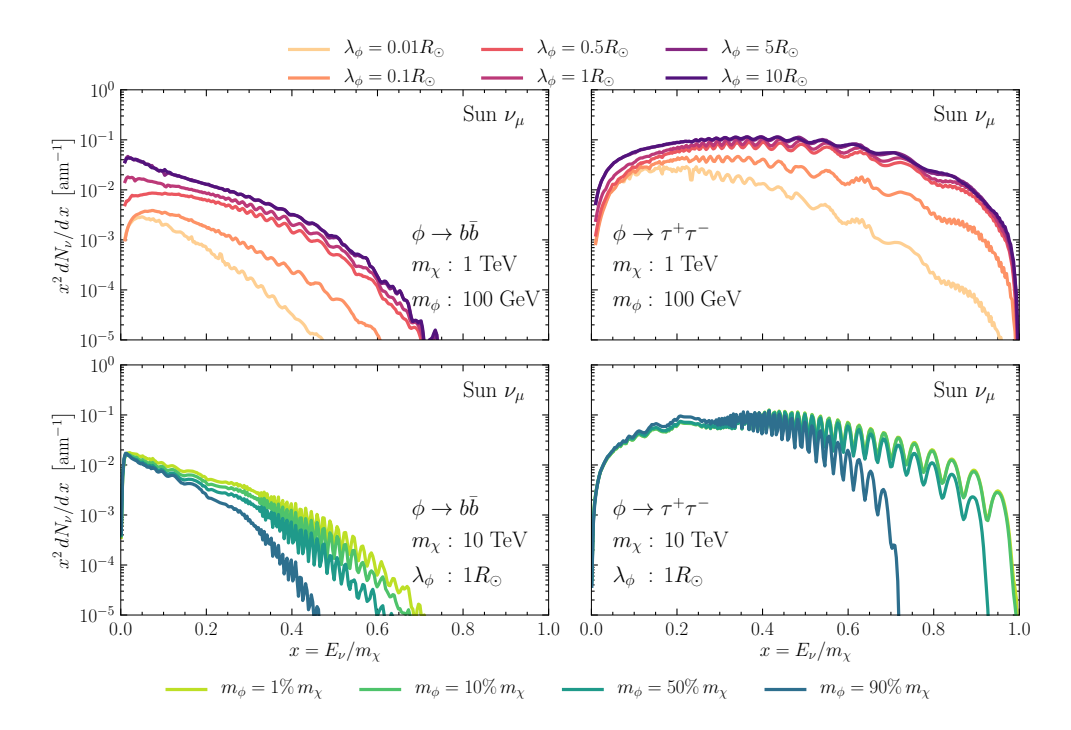


Figure 7. Solar secluded DM neutrino fluxes at 1 AU. In the left panels we show the muon neutrino spectrum for the $b\bar{b}$ channel and in the right panels the $\tau^+\tau^-$ channel. The top plots are meant to illustrate the dependence on the mediator decay length; for this we set the mediator mass to be 100 GeV and the DM mass 1 TeV. The different lines show different mediator decay lengths in units of the solar radius; where they are color-sorted from shortest to longest as they go from lighter to darker. The bottom plots are meant to illustrate the dependence on the mediator mass, for this we now set the decay length to be one solar radius and the DM mass to be 10 TeV. The different lines show different mediator mass, which we show as a fraction of the DM mass; color-sorted from lightest to heaviest as they go from lighter to darker.

of ways. For example, the ratio of m_{ϕ} and m_{χ} affects the angular and energy distributions of the spectrum, since at lower values of this ratio, the mediator will be highly boosted, creating a harder, more collimated spectrum. Furthermore, λ_{ϕ} plays an important role in dense environments because as the decay length grows, the attenuation of final products decreases. If λ_{ϕ} is larger than the radius of the neutrino-opaque environment, e.g. $\lambda_{\phi} > r_{\odot}$ in the Sun, one can additionally look for photons, protons, electrons, and positrons as a DM signature. In this case, the usefulness of e^- and p as messengers is case dependent since interplanetary magnetic fields can bend their trajectories such that they do not point back to their source; however, an excess of high-energy positrons or anti-protons can be a smoking-gun signature for DM [180, 181]. Additionally, the introduction of λ_{ϕ} changes the production region from the point-like production region considered previously to an extended region, with the probability of SM particles being produced at a distance r from the center of the source given by

$$\frac{dP}{dr}(r) = \frac{e^{-r/\lambda_{\phi}}}{\lambda_{\phi}}. (5.1)$$

In order to compute the neutrino spectrum at production, we make use of the previously discussed algorithm with some additional steps that we discuss in the following lines. First, we sample over the production region given by eq. (5.1). Secondly, we allow the DM to

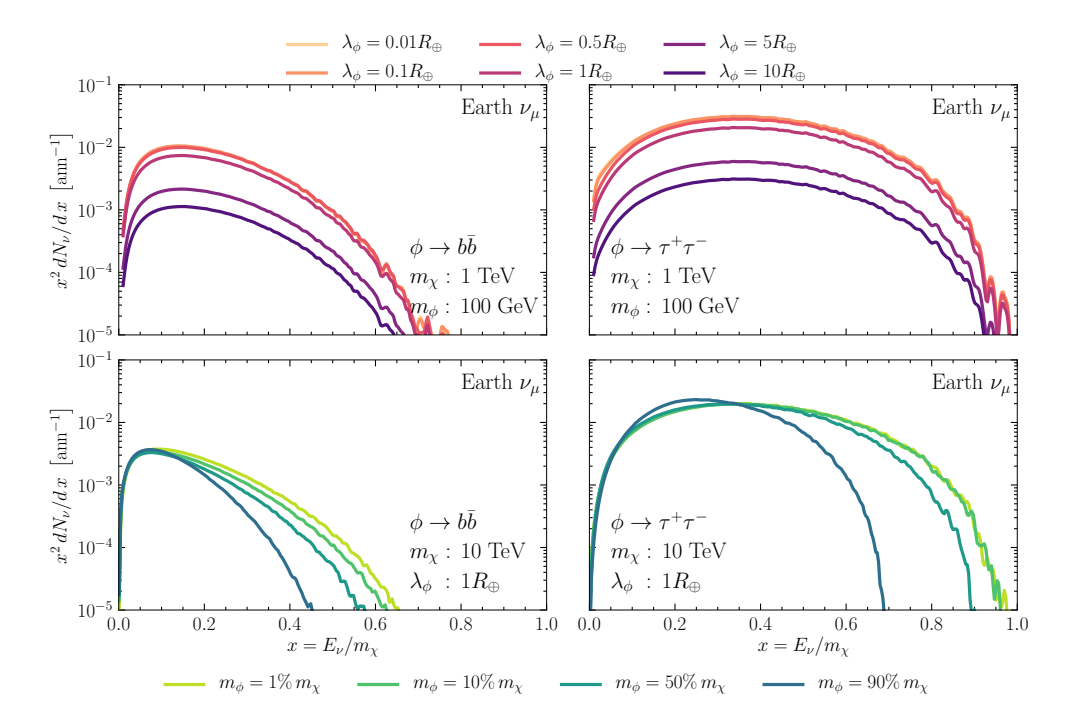


Figure 8. Secluded DM neutrino fluxes from the Earth core at the surface. The layout and format of lines are the same as in figure 7.

decay to the mediator with an initial energy of $m_\chi/2$. We assume that the mediator does not interact on the way from the point of production to the point of decay. Finally, we allow the mediator to decay and collect the energies of all neutrinos produced in the same manner as in the standard case. In this simulation, we include interactions if the decay happens inside the Sun or Earth as discussed in section 3, but with only the EW corrections included in PYTHIA; implementation of the BRW calculation is beyond the scope of this work and will be included in a future version of χ aro ν .

After obtaining the flux throughout the production region, we propagate it to the detector following the process discussed in section 4. In this process, we use the approximation that the final neutrinos are collimated and move in the same direction as the mediator; therefore, we only consider fluxes along the line of sight from the detector to the WIMP decay location. This approximation is valid as long as the mass of the mediator is much smaller than that of the DM; see [182] for a detailed comparison using a three-dimensional simulation. The neutrino yields for secluded DM in the Sun and Earth for a number of choices of λ_{ϕ} and m_{ϕ}/m_{χ} are shown after propagation to the Earth's surface in figures 7 and 8, respectively.

If λ_{ϕ} is small enough that the production region is smaller than the resolution of the detector, the flux can be treated as coming from a point source, and propagation can proceed accordingly; however, if the size of the production region is large than the detector resolution, one must treat this as an extended emission. This requires computing a J-factor along a particular line of sight as described in section 2. This extended source treatment is particularly relevant for the case of secluded DM in the Earth since the distance between the production region and detector is much shorter than in the other cases.

6 Comparison to other calculations and sources of uncertainty

In this section we compare our calculation to other results in the literature and estimate the impact of different sources of uncertainties on the final neutrino flux. For a discussion of QCD uncertainties on particle spectra from showering and hadronisation, see [183]

6.1 Comparison to other calculations

Two broadly used calculations of the flux of neutrinos from DM annihilation or decay have been used in the literature: PPPC and WimpSim. Here, we briefly comment on the differences and similarities between our result and these calculations in the three sources of neutrinos from DM discussed in this work.

First for the standard DM annihilation or decay scenario we have:

- Galactic Center and Halo: DarkSUSY [184, 185], PPPC, or direct Pythia calculation, has been used in results predominantely from DM annihilation from the Galactic Halo, see e.g. results by IceCube [186, 187], ANTARES [187, 188], and Super-Kamiokande [119]. Our calculation using Pythias.2 matches well with previous calculations with Pythia6. Due to the fact that Pythia only partially includes EW interactions both predicted fluxes are smaller than those predicted by PPPC, e.g. the PPPC calculation gives spectra which are ~ 20 times larger for DM annihilation to e^-e^+ with $m_\chi = 1$ TeV. When we incorporate EW corrections, by coupling our calculation with BRW [109], our results yield a flux greater than the Pythia versions, but less than the PPPC calculation by an average factor of 1.8, for the same parameters mentioned above, due to different approaches discussed in section 3.
- Sun: though PPPC provides a calculation of DM annihilation from the Sun, most experimental results use WimpSim. These calculations differ from each other as well as from $\chi aro \nu$ in several meaningful ways, both in their treatment of fluxes at production, and in neutrino transport.

With respect to production, both PPPC and χ aro ν include a treatment of the EW correction, which is not implemented in WimpSim. Furthermore, PPPC handles interactions of stable and metastable particles using Geant4, which tracks low-energy neutrinos produced in interactions of primary hadrons with the environment. These neutrinos are ignored by WimpSim, and as mentioned above, χ aro ν allows the inclusion of these low-energy neutrinos as an option. Lastly, PPPC samples energy losses of b and c hadrons from a distribution, whereas χ aro ν and WimpSim use the average energy loss for a given interaction. Though small, this effect is most notable in hadronic channels, e.g. $b\bar{b}$ [84].

With respect to propagation, both PPPC and ν SQuIDS use an integro-differential equation approach, while WimpSim uses a Monte Carlo based transport. The Monte Carlo approach allows for event-by-event simulation, which offers several advantages. Specifically, it is easier to couple such simulations to detector simulations and allows tracking the position of the Sun on an event-by-event basis. These advantages, however, come at the cost of significantly increasing propagation time. Additionally, the WimpSim calculation uses a neutrino cross section which uses the CTEQ6 parton distribution functions which yields a more accurate cross section than other calculations at small- Q^2 values, e.g. [189] that use HERAPDF. Our calculation is more similar to PPPC

than to WimpSim, and has the following notable differences compared to the latter: we treat DM emission to SM particles as a point-source; we propagate the neutrinos using a differential equation instead of a Monte Carlo method, we take into account the polarization of the τ when considering tau-neutrino regeneration, and, when coupled with BRW calculation [109], have a more complete treatment of EW corrections. As can be seen in figure 9 for a WIMP of 100 GeV our calculation and WimpSim's are in agreement. For DM masses above the EW scale, for definiteness at 10^3 GeV and 10^4 GeV in the figure, our calculation that includes EW corrections is significantly larger than the WimpSim and Pythia-only predictions. In this range the effects can be as large as a factor of four for the $b\bar{b}$ channel with $m_{\chi}=1$ TeV. Lastly, we find the effect of PPPC's partial implementation of EW corrections is channel dependent. For example, in the $b\bar{b}$ channel, PPPC tends to overpredict the flux relative to our calculation over the whole energy range, whereas in the W^+W^- channel PPPC overpredicts the flux at low energies, but underpredicts it at high energies.

• Earth: WimpSim has been used in recent searches for DM annihilation from the Earth, see e.g. results by ANTARES [112], IceCube [113] and Super-Kamiokande [117]. In this case, we find that our results agree well with WimpSim when using PYTHIA to generate the fluxes and are larger when seeding with the BRW [109] calculation as discussed in the Sun case, as expected.

Second for the secluded DM scenario:

- Sun: this scenario was implemented in WimpSim in [182]. Beyond the differences already discussed between WimpSim and $\chi aro \nu$, it should be noted that our implementation of secluded DM is a one-dimensional calculation. In [182], a comparison with a three-dimensional implementation is performed, concluding that effect is only important when the mediator mass, m_{ϕ} , is close to the DM mass, m_{χ} . This causes the products of the mediator not to be collinear with the DM direction and has a 28% effect on average on the final flux when the mediator mass is 98% of the DM mass. For dark mediator mass fractions considered in this work this effect is negligible, and our calculations are in good agreement as can be seen in figure 10. Additionally, if the decay of the mediator is in or near the detector, a di-muon signature from the muon decay channel would be induced, creating a smoking-gun signature of DM [176, 178, 182].
- Earth: the secluded DM scenario has not been implemented in any previous result and is included for the first time in $\chi aro \nu$. Considering this scenario in the Earth is interesting for several reasons. Long-range interactions can induce Sommerfeld-enhanced annihilation cross sections [190, 191]. Similar to the solar case, if the mediator decays to muons and it happens near the detector, it induces a di-muon signature from the direction of the core [176], which is complementary to the neutrino flux predicted here.

6.2 Effects of the neutrino oscillation parameters

To estimate the effect that uncertainties on the neutrino oscillation parameters have on the neutrino yields, we construct a two-sided Gaussian for each parameter centered on the best-fit point from NuFit-4.1 [172], whose standard deviations are the $\pm 1\sigma$ values from the same work. We then sample from each Gaussian independently, and run χ aro ν using the

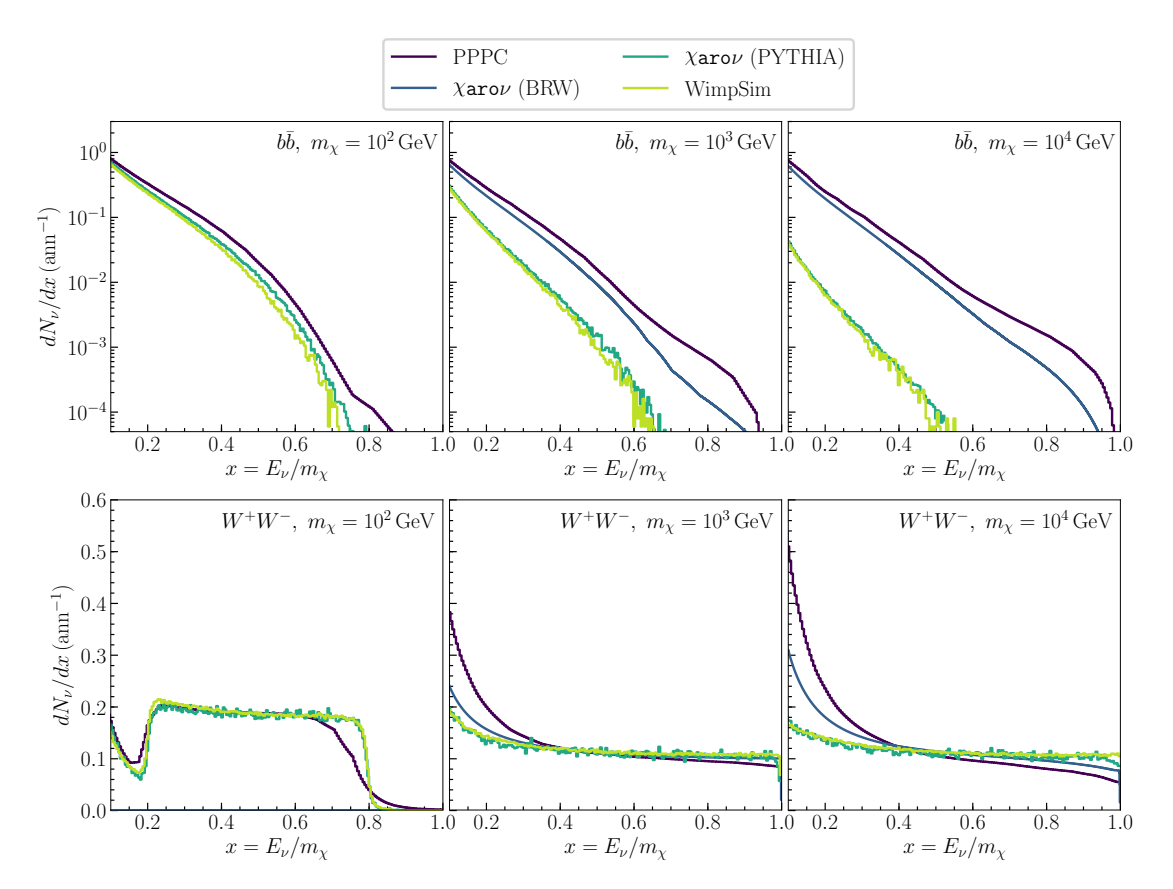


Figure 9. Comparison of ν_{μ} -yield using four different signal generators for DM at the Sun center. The major contribution to differences between the lines is that a more complete treatment of the EW correction has been implemented in PPPC and $\chi_{aro\nu}$ (BRW). As expected, the magnitude of this difference grows as the mass of the DM increases. When comparing the PYTHIA-based calculations, the $b\bar{b}$ channel in $\chi_{aro\nu}$ is slightly harder than WimpSim which is consistent with the result from [52]. The BRW calculation does not extend to masses below 500 GeV and so it is absent from the first column.

resulting parameters. We repeat this procedure to create a distribution of fluxes, and create the highest-density posterior interval at given credible levels.

The results of this procedure at the 2σ level are shown for $\chi\chi \to W^+W^-$ and $m_{\chi} = 10^3 \,\text{GeV}$ in figure 11, where this is performed separately for normal and inverted ordering. The uncertainty 95% containment region gives an uncertainty of up to 15% at energies below $\sim 200 \,\text{GeV}$, with these differences shrinking to a few percent for higher energy neutrinos.

6.3 Effects of the neutrino cross section

To estimate the effect that cross section uncertainties have on the neutrino flux, we follow a procedure similar to the previously discussed procedure. In this case, however, we construct a two-sided Gaussian centered around one, and the sigma values are the percent uncertainty given in [189], using the central value from this same work, which we assume to be comparable to the NuSigma cross sections. We then sample from these distributions at each energy, and rescale the default ν SQuIDS cross section by the drawn value. We repeat this procedure to create a distribution of fluxes, and create the highest-density posterior interval at given credible levels. The result of this procedure is shown in 12.

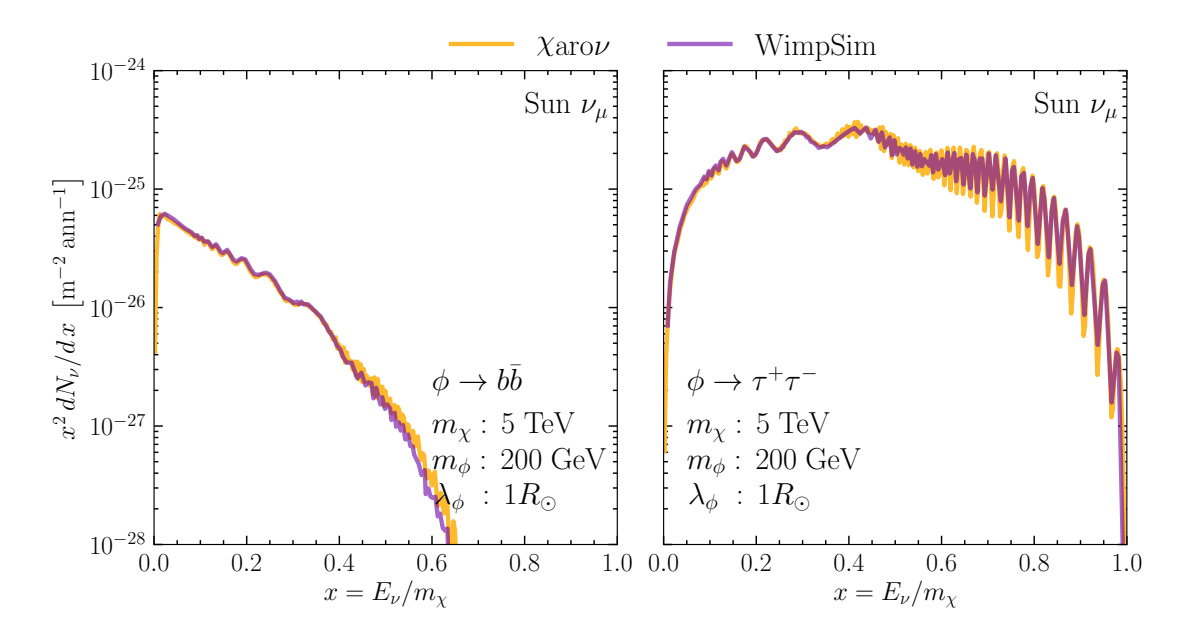


Figure 10. Comparison of χ arov and WimpSim for the solar secluded case. The WimpSim fluxes are from [182] and oscillation parameters have been set to be the same values. The two fluxes are in good agreement. The tail of $b\bar{b}$ channel of χ arov is slightly harder than of WimpSim, in agreement with our observed difference between these two calculations in the standard scenario. The difference of the oscillating amplitude is from interpolation which is affected by binning.

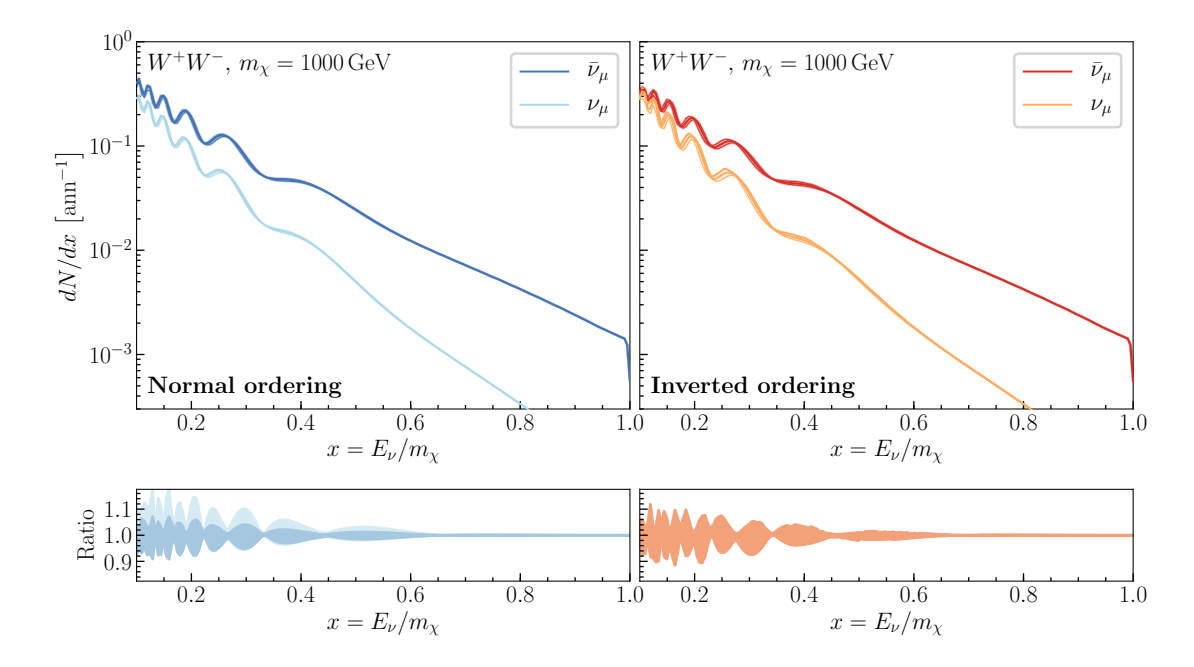


Figure 11. Effects of oscillation parameters and neutrino ordering. We vary each oscillation parameter according to the procedure described in the text. In both panels we assume annihilation to W^+W^- with $m_\chi=1\,\mathrm{TeV}$; on the left plot we assume normal neutrino ordering and on the right one inverted ordering. The envelopes show the 2σ uncertainty regions.

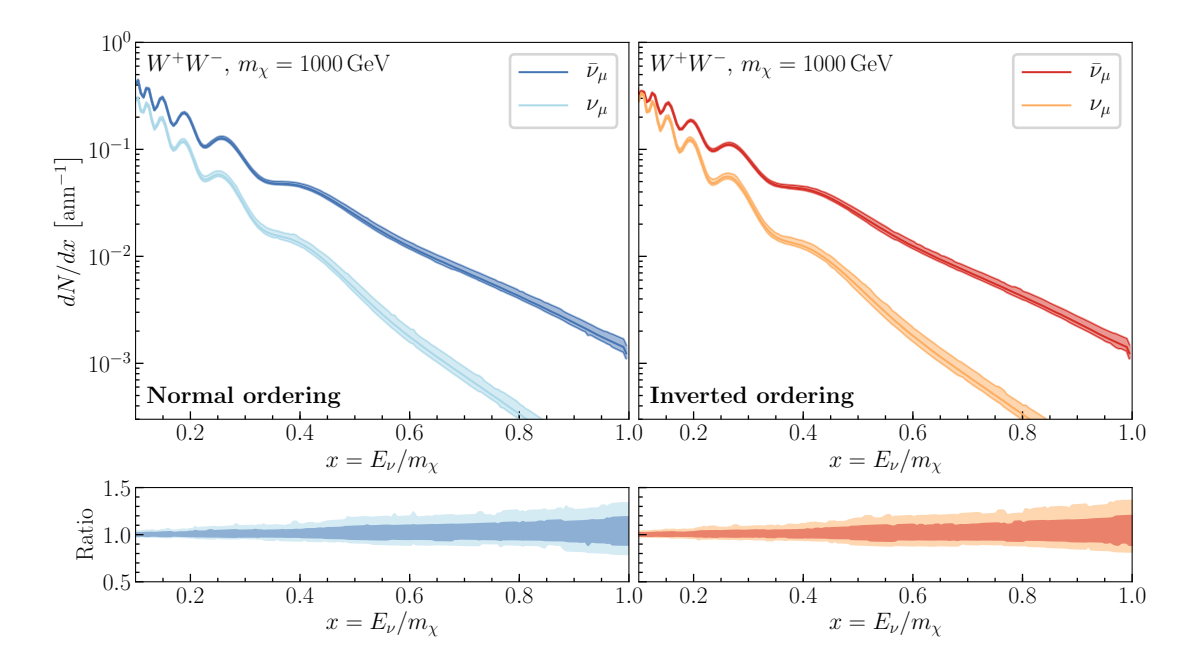


Figure 12. Effects of the neutrino cross section uncertainties. We vary cross sections according to the procedure described in the text. In both panels we assume annihilation to W^+W^- with $m_{\chi} = 1 \text{ TeV}$; on the left plot we assume normal neutrino ordering and on the right one inverted ordering. We use the CSMS cross section model [189], and show the 2σ using the uncertainties from this work.

The effect of cross section uncertainties is quite small at low energies as the opacity is small at these energies, but it grows with energy. At the highest energies, the error on the flux reaches $\sim 50\%$ for ν_{μ} and $\sim 25\%$ for $\bar{\nu}_{\mu}$. The reason for the increasing uncertainty can be understood from the fact that the survival probability, $p_{\rm sur.}$, is given by $\exp{(-n\sigma(E_{\nu}))}$, where n is total column density traversed and $\sigma(E_{\nu})$ the total cross section at a given neutrino energy, E_{ν} . This implies that the relative uncertainty is $\delta\left[p_{\rm sur.}\right]/p_{\rm sur.} \propto \delta\left[\sigma(E_{\nu})\right]$, which increases with energy.

7 Conclusion

In this work we have computed the flux of neutrinos from DM decay and annihilation both in the standard WIMP paradigm as well as in the secluded DM scenario. Our calculation includes several updates over previous results such as new EW corrections for neutrino production using the BRW calculation [109], as well as a new propagation tool that is flexible and allows one to vary parameters, such as the neutrino oscillation parameters and neutrino-nucleon cross sections. Additionally, we include the possibility of the secluded DM scenario in the Sun and Earth, the latter of which is a new result. In our new result we find that, when including EW corrections consistently, the flux of neutrinos from DM annihilation or decay for DM masses above the EW scale is increased by a factor of ~ 2 for 500 GeV and ~ 100 for 10 TeV for $b\bar{b}$ channel on average. Since the effect of this, in the range where neutrinos are able to exit their production environment, is to approximately rescale the flux, current constraints on DM annihilation from the Sun and Earth are underestimated by approximately this same factor.

Acknowledgments

We thank Marco Cirelli, Joakim Edsjö and Francis Halzen for useful discussions. We also thank Christian Bauer, Nicholas Rodd, and Bryan Webber for a fruitful collaboration. We thank Peter Denton, Alejandro Diaz, Matheus Hostert, Zach Krebs, Ibrahim Safa, and Carsten Rott for comments on the draft. We would like to give special thanks to Sergio Palomares-Ruiz and Aaron Vincent for their detailed comments that have greatly improved this work. CAA was supported by NSF grant PHY-1912764. AK acknowledges the support from the IGC Postdoctoral Award. QL and JL are supported by NSF under grants PLR-1600823 and PHY-1607644 and by the University of Wisconsin Research Council with funds granted by the Wisconsin Alumni Research Foundation.

References

- [1] Particle Data Group collaboration, Review of particle physics, Phys. Rev. D 98 (2018) 030001 [INSPIRE].
- [2] I. Esteban, M.C. Gonzalez-Garcia, A. Hernandez-Cabezudo, M. Maltoni and T. Schwetz, Global analysis of three-flavour neutrino oscillations: synergies and tensions in the determination of θ_{23} , δ_{CP} , and the mass ordering, JHEP **01** (2019) 106 [arXiv:1811.05487] [INSPIRE].
- [3] J.N. Bahcall, S. Basu and M.H. Pinsonneault, How uncertain are solar neutrino predictions?, Phys. Lett. B 433 (1998) 1 [astro-ph/9805135] [INSPIRE].
- [4] J.N. Bahcall, A.M. Serenelli and S. Basu, New solar opacities, abundances, helioseismology, and neutrino fluxes, Astrophys. J. Lett. **621** (2005) L85 [astro-ph/0412440] [INSPIRE].
- [5] R. Davis, A review of the Homestake solar neutrino experiment, Prog. Part. Nucl. Phys. 32 (1994) 13 [INSPIRE].
- [6] J.N. Bahcall, Solving the mystery of the missing neutrinos, physics/0406040 [INSPIRE].
- [7] A.J. Lowe, Neutrino physics and the solar neutrino problem, arXiv:0907.3658 [INSPIRE].
- [8] J.N. Bahcall, M.C. Gonzalez-Garcia and C. Pena-Garay, Does the sun shine by pp or CNO fusion reactions?, Phys. Rev. Lett. 90 (2003) 131301 [astro-ph/0212331] [INSPIRE].
- [9] J.N. Bahcall, P.I. Krastev and A. Smirnov, Is large mixing angle MSW the solution of the solar neutrino problems?, Phys. Rev. D 60 (1999) 093001 [hep-ph/9905220] [INSPIRE].
- [10] F. Zwicky, On the masses of nebulae and of clusters of nebulae, Astrophys. J. 86 (1937) 271.
- [11] F.D. Kahn and L. Woltjer, Intergalactic matter and the galaxy, Astrophys. J. 130 (1959) 705.
- [12] K.C. Freeman, On the disks of spiral and SO Galaxies, Astrophys. J. 160 (1970) 811 [INSPIRE].
- [13] D.H. Rogstad and G.S. Shostak, Gross properties of five scd galaxies as determined from 21-centimeter observations, Astrophys. J. 176 (1972) 315
- [14] J.I. Read, The local dark matter density, J. Phys. G 41 (2014) 063101 [arXiv:1404.1938] [INSPIRE].
- [15] Planck collaboration, Planck 2018 results. VI. Cosmological parameters, Astron. Astrophys.
 641 (2020) A6 [arXiv:1807.06209] [INSPIRE].
- [16] E. Ma, Verifiable radiative seesaw mechanism of neutrino mass and dark matter, Phys. Rev. D 73 (2006) 077301 [hep-ph/0601225] [INSPIRE].

- [17] C. Boehm, Y. Farzan, T. Hambye, S. Palomares-Ruiz and S. Pascoli, *Is it possible to explain neutrino masses with scalar dark matter?*, *Phys. Rev. D* **77** (2008) 043516 [hep-ph/0612228] [INSPIRE].
- [18] Y. Farzan and E. Ma, Dirac neutrino mass generation from dark matter, Phys. Rev. D 86 (2012) 033007 [arXiv:1204.4890] [INSPIRE].
- [19] M. Escudero, N. Rius and V. Sanz, Sterile neutrino portal to dark matter. Part I. The $U(1)_{B-L}$ case, JHEP **02** (2017) 045 [arXiv:1606.01258] [INSPIRE].
- [20] M. Escudero, N. Rius and V. Sanz, Sterile neutrino portal to dark matter. Part II. Exact dark symmetry, Eur. Phys. J. C 77 (2017) 397 [arXiv:1607.02373] [INSPIRE].
- [21] J.B.G. Alvey and M. Fairbairn, Linking scalar dark matter and neutrino masses with IceCube 170922A, JCAP 07 (2019) 041 [arXiv:1902.01450] [INSPIRE].
- [22] P. Ballett, M. Hostert and S. Pascoli, Neutrino masses from a dark neutrino sector below the electroweak scale, Phys. Rev. D 99 (2019) 091701 [arXiv:1903.07590] [INSPIRE].
- [23] P. Ballett, M. Hostert and S. Pascoli, Dark neutrinos and a three portal connection to the standard model, Phys. Rev. D 101 (2020) 115025 [arXiv:1903.07589] [INSPIRE].
- [24] A. Abdullahi, M. Hostert and S. Pascoli, A dark seesaw solution to low energy anomalies: MiniBooNE, the muon (g-2), and BaBar, arXiv:2007.11813 [INSPIRE].
- [25] K.-Y. Choi, E.J. Chun and J. Kim, Neutrino oscillations in dark matter, Phys. Dark Univ. 30 (2020) 100606 [arXiv:1909.10478] [INSPIRE].
- [26] A. Abada, G. Arcadi and M. Lucente, *Dark matter in the minimal inverse seesaw mechanism*, JCAP 10 (2014) 001 [arXiv:1406.6556] [INSPIRE].
- [27] S. Bhattacharya, I. de Medeiros Varzielas, B. Karmakar, S.F. King and A. Sil, *Dark side of the seesaw*, *JHEP* **12** (2018) 007 [arXiv:1806.00490] [INSPIRE].
- [28] M. Chianese and S.F. King, The dark side of the littlest seesaw: freeze-in, the two right-handed neutrino portal and leptogenesis-friendly fimpzillas, JCAP **09** (2018) 027 [arXiv:1806.10606] [INSPIRE].
- [29] J. Silk, K.A. Olive and M. Srednicki, *The photino*, the Sun and high-energy neutrinos, *Phys. Rev. Lett.* **55** (1985) 257 [INSPIRE].
- [30] J.S. Hagelin, K.W. Ng and K.A. Olive, A high-energy neutrino signature from supersymmetric relics, Phys. Lett. B 180 (1986) 375 [INSPIRE].
- [31] T.K. Gaisser, G. Steigman and S. Tilav, Limits on cold dark matter candidates from deep underground detectors, Phys. Rev. D 34 (1986) 2206 [INSPIRE].
- [32] M. Srednicki, K.A. Olive and J. Silk, High-energy neutrinos from the Sun and cold dark matter, Nucl. Phys. B 279 (1987) 804 [INSPIRE].
- [33] K. Griest and D. Seckel, Cosmic asymmetry, neutrinos and the Sun, Nucl. Phys. B **283** (1987) 681 [Erratum ibid. **296** (1988) 1034] [INSPIRE].
- [34] I.V. Moskalenko and S. Karakula, Very high-energy neutrinos from the sun, J. Phys. G 19 (1993) 1399 [INSPIRE].
- [35] G. Ingelman and M. Thunman, *High-energy neutrino production by cosmic ray interactions in the sun*, *Phys. Rev. D* **54** (1996) 4385 [hep-ph/9604288] [INSPIRE].
- [36] C. Hettlage, K. Mannheim and J.G. Learned, *The Sun as a high-energy neutrino source*, Astropart. Phys. **13** (2000) 45 [astro-ph/9910208] [INSPIRE].
- [37] C. Argüelles, G. de Wasseige, A. Fedynitch and B.P. Jones, Solar atmospheric neutrinos and the sensitivity floor for solar dark matter annihilation searches, JCAP **07** (2017) 024 [arXiv:1703.07798] [INSPIRE].

- [38] J. Edsjo, J. Elevant, R. Enberg and C. Niblaeus, Neutrinos from cosmic ray interactions in the Sun, JCAP 06 (2017) 033 [arXiv:1704.02892] [INSPIRE].
- [39] K.C.Y. Ng, J.F. Beacom, A.H.G. Peter and C. Rott, Solar atmospheric neutrinos: a new neutrino floor for dark matter searches, Phys. Rev. D 96 (2017) 103006 [arXiv:1703.10280] [INSPIRE].
- [40] ICECUBE collaboration, Searches for neutrinos from cosmic-ray interactions in the Sun using seven years of IceCube data, arXiv:1912.13135 [INSPIRE].
- [41] M. Kamionkowski, Energetic neutrinos from heavy neutralino annihilation in the sun, Phys. Rev. D 44 (1991) 3021 [INSPIRE].
- [42] A. Bottino, V. de Alfaro, N. Fornengo, G. Mignola and M. Pignone, *Indirect search for neutralinos at neutrino telescopes*, *Phys. Lett. B* **265** (1991) 57 [INSPIRE].
- [43] F. Halzen, T. Stelzer and M. Kamionkowski, Signatures of dark matter in underground detectors, Phys. Rev. D 45 (1992) 4439 [INSPIRE].
- [44] R. Gandhi, J.L. Lopez, D.V. Nanopoulos, K.-j. Yuan and A. Zichichi, Scrutinizing supergravity models through neutrino telescopes, Phys. Rev. D 49 (1994) 3691 [astro-ph/9309048] [INSPIRE].
- [45] A. Bottino, N. Fornengo, G. Mignola and L. Moscoso, Signals of neutralino dark matter from earth and sun, Astropart. Phys. 3 (1995) 65 [hep-ph/9408391] [INSPIRE].
- [46] L. Bergstrom, J. Edsjo and P. Gondolo, Indirect neutralino detection rates in neutrino telescopes, Phys. Rev. D 55 (1997) 1765 [hep-ph/9607237] [INSPIRE].
- [47] L. Bergstrom, J. Edsjo and P. Gondolo, *Indirect detection of dark matter in KM size neutrino telescopes*, *Phys. Rev. D* **58** (1998) 103519 [hep-ph/9806293] [INSPIRE].
- [48] V.D. Barger, F. Halzen, D. Hooper and C. Kao, *Indirect search for neutralino dark matter with high-energy neutrinos*, *Phys. Rev. D* **65** (2002) 075022 [hep-ph/0105182] [INSPIRE].
- [49] V. Bertin, E. Nezri and J. Orloff, Neutrino indirect detection of neutralino dark matter in the CMSSM, Eur. Phys. J. C 26 (2002) 111 [hep-ph/0204135] [INSPIRE].
- [50] D. Hooper and G.D. Kribs, *Probing Kaluza-Klein dark matter with neutrino telescopes*, *Phys. Rev. D* **67** (2003) 055003 [hep-ph/0208261] [INSPIRE].
- [51] A. Bueno, R. Cid, S. Navas, D. Hooper and T.J. Weiler, *Indirect detection of dark matter WIMPs in a liquid argon TPC*, *JCAP* **01** (2005) 001 [hep-ph/0410206] [INSPIRE].
- [52] M. Cirelli, N. Fornengo, T. Montaruli, I.A. Sokalski, A. Strumia and F. Vissani, Spectra of neutrinos from dark matter annihilations, Nucl. Phys. B 727 (2005) 99 [Erratum ibid. 790 (2008) 338] [hep-ph/0506298] [INSPIRE].
- [53] F. Halzen and D. Hooper, Prospects for detecting dark matter with neutrino telescopes in light of recent results from direct detection experiments, Phys. Rev. D 73 (2006) 123507 [hep-ph/0510048] [INSPIRE].
- [54] O. Mena, S. Palomares-Ruiz and S. Pascoli, Reconstructing WIMP properties with neutrino detectors, Phys. Lett. B 664 (2008) 92 [arXiv:0706.3909] [INSPIRE].
- [55] R. Lehnert and T.J. Weiler, Neutrino flavor ratios as diagnostic of solar WIMP annihilation, Phys. Rev. D 77 (2008) 125004 [arXiv:0708.1035] [INSPIRE].
- [56] V. Barger, W.-Y. Keung, G. Shaughnessy and A. Tregre, High energy neutrinos from neutralino annihilations in the Sun, Phys. Rev. D 76 (2007) 095008 [arXiv:0708.1325] [INSPIRE].
- [57] V.D. Barger, W.-Y. Keung and G. Shaughnessy, Monochromatic neutrino signals from dark matter annihilation, Phys. Lett. B 664 (2008) 190 [arXiv:0709.3301] [INSPIRE].

- [58] M. Blennow, J. Edsjo and T. Ohlsson, Neutrinos from WIMP annihilations using a full three-flavor Monte Carlo, JCAP 01 (2008) 021 [arXiv:0709.3898] [INSPIRE].
- [59] J. Liu, P.-f. Yin and S.-h. Zhu, Neutrino signals from solar neutralino annihilations in anomaly mediated supersymmetry breaking model, Phys. Rev. D 77 (2008) 115014 [arXiv:0803.2164] [INSPIRE].
- [60] D. Hooper, F. Petriello, K.M. Zurek and M. Kamionkowski, The new DAMA dark-matter window and energetic-neutrino searches, Phys. Rev. D 79 (2009) 015010 [arXiv:0808.2464] [INSPIRE].
- [61] G. Wikstrom and J. Edsjo, Limits on the WIMP-nucleon scattering cross-section from neutrino telescopes, JCAP 04 (2009) 009 [arXiv:0903.2986] [INSPIRE].
- [62] S. Nussinov, L.-T. Wang and I. Yavin, Capture of inelastic dark matter in the Sun, JCAP 08 (2009) 037 [arXiv:0905.1333] [INSPIRE].
- [63] A. Menon, R. Morris, A. Pierce and N. Weiner, Capture and indirect detection of inelastic dark matter, Phys. Rev. D 82 (2010) 015011 [arXiv:0905.1847] [INSPIRE].
- [64] M.R. Buckley, K. Freese, D. Hooper, D. Spolyar and H. Murayama, High-energy neutrino signatures of dark matter decaying into leptons, Phys. Rev. D 81 (2010) 016006 [arXiv:0907.2385] [INSPIRE].
- [65] A.R. Zentner, High-energy neutrinos from dark matter particle self-capture within the Sun, Phys. Rev. D 80 (2009) 063501 [arXiv:0907.3448] [INSPIRE].
- [66] J. Ellis, K.A. Olive, C. Savage and V.C. Spanos, Neutrino Fluxes from CMSSM LSP annihilations in the Sun, Phys. Rev. D 81 (2010) 085004 [arXiv:0912.3137] [INSPIRE].
- [67] A. Esmaili and Y. Farzan, On the oscillation of neutrinos produced by the annihilation of dark matter inside the Sun, Phys. Rev. D 81 (2010) 113010 [arXiv:0912.4033] [INSPIRE].
- [68] J. Ellis, K.A. Olive, C. Savage and V.C. Spanos, Neutrino fluxes from NUHM LSP annihilations in the Sun, Phys. Rev. D 83 (2011) 085023 [arXiv:1102.1988] [INSPIRE].
- [69] N.F. Bell and K. Petraki, Enhanced neutrino signals from dark matter annihilation in the Sun via metastable mediators, JCAP 04 (2011) 003 [arXiv:1102.2958] [INSPIRE].
- [70] R. Kappl and M.W. Winkler, New limits on dark matter from super-Kamiokande, Nucl. Phys. B 850 (2011) 505 [arXiv:1104.0679] [INSPIRE].
- [71] S.K. Agarwalla, M. Blennow, E. Fernandez Martinez and O. Mena, Neutrino probes of the nature of light dark matter, JCAP 09 (2011) 004 [arXiv:1105.4077] [INSPIRE].
- [72] S.-L. Chen and Y. Zhang, Isospin-violating dark matter and neutrinos from the Sun, Phys. Rev. D 84 (2011) 031301 [arXiv:1106.4044] [INSPIRE].
- [73] S. Kundu and P. Bhattacharjee, Neutrinos from WIMP annihilation in the Sun: implications of a self-consistent model of the Milky Way's dark matter halo, Phys. Rev. D 85 (2012) 123533 [arXiv:1106.5711] [INSPIRE].
- [74] C. Rott, T. Tanaka and Y. Itow, Enhanced sensitivity to dark matter self-annihilations in the Sun using neutrino spectral information, JCAP **09** (2011) 029 [arXiv:1107.3182] [INSPIRE].
- [75] C.R. Das, O. Mena, S. Palomares-Ruiz and S. Pascoli, Determining the dark matter mass with DeepCore, Phys. Lett. B 725 (2013) 297 [arXiv:1110.5095] [INSPIRE].
- [76] J. Kumar, J.G. Learned, S. Smith and K. Richardson, Tools for studying low-mass dark matter at neutrino detectors, Phys. Rev. D 86 (2012) 073002 [arXiv:1204.5120] [INSPIRE].
- [77] N.F. Bell, A.J. Brennan and T.D. Jacques, Neutrino signals from electroweak bremsstrahlung in solar WIMP annihilation, JCAP 10 (2012) 045 [arXiv:1206.2977] [INSPIRE].

- [78] H. Silverwood, P. Scott, M. Danninger, C. Savage, J. Edsjö, J. Adams et al., Sensitivity of IceCube-DeepCore to neutralino dark matter in the MSSM-25, JCAP 03 (2013) 027 [arXiv:1210.0844] [INSPIRE].
- [79] M. Blennow, M. Carrigan and E. Fernandez Martinez, *Probing the dark matter mass and nature with neutrinos*, *JCAP* **06** (2013) 038 [arXiv:1303.4530] [INSPIRE].
- [80] C. Arina, G. Bertone and H. Silverwood, Complementarity of direct and indirect dark matter detection experiments, Phys. Rev. D 88 (2013) 013002 [arXiv:1304.5119] [INSPIRE].
- [81] Z.-L. Liang and Y.-L. Wu, Direct detection and solar capture of spin-dependent dark matter, Phys. Rev. D 89 (2014) 013010 [arXiv:1308.5897] [INSPIRE].
- [82] A. Ibarra, M. Totzauer and S. Wild, *High-energy neutrino signals from the Sun in dark matter scenarios with internal bremsstrahlung*, *JCAP* 12 (2013) 043 [arXiv:1311.1418] [INSPIRE].
- [83] I.F.M. Albuquerque, C. Pérez de Los Heros and D.S. Robertson, Constraints on self interacting dark matter from IceCube results, JCAP 02 (2014) 047 [arXiv:1312.0797] [INSPIRE].
- [84] P. Baratella, M. Cirelli, A. Hektor, J. Pata, M. P IIBeleht and A. Strumia, *PPPC 4 DMν: a poor particle physicist cookbook for neutrinos from dark matter annihilations in the Sun*, *JCAP* **03** (2014) 053 [arXiv:1312.6408] [INSPIRE].
- [85] W.-L. Guo, Z.-L. Liang and Y.-L. Wu, Direct detection and solar capture of dark matter with momentum and velocity dependent elastic scattering, Nucl. Phys. B 878 (2014) 295 [arXiv:1305.0912] [INSPIRE].
- [86] A. Ibarra, M. Totzauer and S. Wild, Higher order dark matter annihilations in the Sun and implications for IceCube, JCAP 04 (2014) 012 [arXiv:1402.4375] [INSPIRE].
- [87] C.-S. Chen, F.-F. Lee, G.-L. Lin and Y.-H. Lin, Probing dark matter self-interaction in the Sun with IceCube-PINGU, JCAP 10 (2014) 049 [arXiv:1408.5471] [INSPIRE].
- [88] J. Blumenthal, P. Gretskov, M. Krämer and C. Wiebusch, Effective field theory interpretation of searches for dark matter annihilation in the Sun with the IceCube Neutrino Observatory, Phys. Rev. D 91 (2015) 035002 [arXiv:1411.5917] [INSPIRE].
- [89] R. Catena, Dark matter signals at neutrino telescopes in effective theories, JCAP **04** (2015) 052 [arXiv:1503.04109] [INSPIRE].
- [90] J. Chen, Z.-L. Liang, Y.-L. Wu and Y.-F. Zhou, Long-range self-interacting dark matter in the Sun, JCAP 12 (2015) 021 [arXiv:1505.04031] [INSPIRE].
- [91] G. Bélanger, J. Da Silva, T. Perrillat-Bottonet and A. Pukhov, Limits on dark matter proton scattering from neutrino telescopes using MicrOMEGAs, JCAP 12 (2015) 036 [arXiv:1507.07987] [INSPIRE].
- [92] J. Heisig, M. Krämer, M. Pellen and C. Wiebusch, Constraints on Majorana Dark Matter from the LHC and IceCube, Phys. Rev. D 93 (2016) 055029 [arXiv:1509.07867] [INSPIRE].
- [93] M. Danninger and C. Rott, Solar WIMPs unravelled: experiments, astrophysical uncertainties, and interactive tools, Phys. Dark Univ. 5-6 (2014) 35 [arXiv:1509.08230] [INSPIRE].
- [94] M. Blennow, S. Clementz and J. Herrero-Garcia, Pinning down inelastic dark matter in the Sun and in direct detection, JCAP 04 (2016) 004 [arXiv:1512.03317] [INSPIRE].
- [95] K. Murase and I.M. Shoemaker, Detecting asymmetric dark matter in the Sun with Neutrinos, Phys. Rev. D 94 (2016) 063512 [arXiv:1606.03087] [INSPIRE].
- [96] J. Lopes and I. Lopes, New limits on thermally annihilating dark matter from neutrino telescopes, Astrophys. J. 827 (2016) 130 [arXiv:1607.08672] [INSPIRE].
- [97] S. Baum, L. Visinelli, K. Freese and P. Stengel, Dark matter capture, subdominant WIMPs, and neutrino observatories, Phys. Rev. D 95 (2017) 043007 [arXiv:1611.09665] [INSPIRE].

- [98] R. Allahverdi, Y. Gao, B. Knockel and S. Shalgar, Indirect signals from solar dark matter annihilation to long-lived right-handed neutrinos, Phys. Rev. D 95 (2017) 075001 [arXiv:1612.03110] [INSPIRE].
- [99] C. Rott, J. Siegal-Gaskins and J.F. Beacom, New sensitivity to solar WIMP annihilation using low-energy neutrinos, Phys. Rev. D 88 (2013) 055005 [arXiv:1208.0827] [INSPIRE].
- [100] N. Bernal, J. Martín-Albo and S. Palomares-Ruiz, A novel way of constraining WIMPs annihilations in the Sun: MeV neutrinos, JCAP 08 (2013) 011 [arXiv:1208.0834] [INSPIRE].
- [101] C. Rott, S. In, J. Kumar and D. Yaylali, Dark matter searches for monoenergetic neutrinos arising from stopped meson decay in the Sun, JCAP 11 (2015) 039 [arXiv:1510.00170] [INSPIRE].
- [102] C. Rott, S. In, J. Kumar and D. Yaylali, Directional searches at DUNE for sub-GeV monoenergetic neutrinos arising from dark matter annihilation in the Sun, JCAP **01** (2017) 016 [arXiv:1609.04876] [INSPIRE].
- [103] ANTARES collaboration, Limits on dark matter annihilation in the Sun using the ANTARES neutrino telescope, Phys. Lett. B 759 (2016) 69 [arXiv:1603.02228] [INSPIRE].
- [104] Baikal collaboration, Search for neutrino emission from relic dark matter in the Sun with the Baikal NT200 detector, Astropart. Phys. 62 (2015) 12 [arXiv:1405.3551] [INSPIRE].
- [105] M.M. Boliev, S.V. Demidov, S.P. Mikheyev and O.V. Suvorova, Search for muon signal from dark matter annihilations in the Sun with the Baksan Underground Scintillator Telescope for 24.12 years, JCAP 09 (2013) 019 [arXiv:1301.1138] [INSPIRE].
- [106] ICECUBE collaboration, Search for annihilating dark matter in the Sun with 3 years of IceCube data, Eur. Phys. J. C 77 (2017) 146 [Erratum ibid. 79 (2019) 214] [arXiv:1612.05949] [INSPIRE].
- [107] SUPER-KAMIOKANDE collaboration, Search for dark matter WIMPs using upward through-going muons in Super-Kamiokande, Phys. Rev. D 70 (2004) 083523 [Erratum ibid. 70 (2004) 109901] [hep-ex/0404025] [INSPIRE].
- [108] SUPER-KAMIOKANDE collaboration, Search for neutrinos from annihilation of captured low-mass dark matter particles in the Sun by Super-Kamiokande, Phys. Rev. Lett. 114 (2015) 141301 [arXiv:1503.04858] [INSPIRE].
- [109] C.W. Bauer, N.L. Rodd and B.R. Webber, Dark matter spectra from the electroweak to the Planck scale, arXiv:2007.15001 [INSPIRE].
- [110] L.M. Krauss, M. Srednicki and F. Wilczek, Solar system constraints and signatures for dark matter candidates, Phys. Rev. D 33 (1986) 2079 [INSPIRE].
- [111] K. Freese, Can scalar neutrinos or massive Dirac neutrinos be the missing mass?, Phys. Lett. B 167 (1986) 295 [INSPIRE].
- [112] ANTARES collaboration, Search for dark matter annihilation in the Earth using the ANTARES Neutrino Telescope, Phys. Dark Univ. 16 (2017) 41 [arXiv:1612.06792] [INSPIRE].
- [113] ICECUBE collaboration, First search for dark matter annihilations in the Earth with the IceCube detector, Eur. Phys. J. C 77 (2017) 82 [arXiv:1609.01492] [INSPIRE].
- [114] ICECUBE collaboration, IceCube search for dark matter annihilation in nearby galaxies and galaxy clusters, Phys. Rev. D 88 (2013) 122001 [arXiv:1307.3473] [INSPIRE].
- [115] ICECUBE collaboration, Search for dark matter annihilation in the Galactic Center with IceCube-79, Eur. Phys. J. C 75 (2015) 492 [arXiv:1505.07259] [INSPIRE].

- [116] BAIKAL collaboration, A search for neutrino signal from dark matter annihilation in the center of the Milky Way with Baikal NT200, Astropart. Phys. 81 (2016) 12 [arXiv:1512.01198] [INSPIRE].
- [117] SUPER-KAMIOKANDE collaboration, Dark matter searches with the Super-Kamiokande detector, J. Phys. Conf. Ser. 888 (2017) 012210 [INSPIRE].
- [118] ICECUBE collaboration, Combined Search for Neutrinos from Dark Matter Annihilation in the Galactic Centre using ANTARES and IceCube, PoS(ICRC2019)522 [arXiv:1908.07300] [INSPIRE].
- [119] SUPER-KAMIOKANDE collaboration, Indirect search for dark matter from the Galactic Center and halo with the Super-Kamiokande detector, arXiv:2005.05109 [INSPIRE].
- [120] S. Palomares-Ruiz, Review of indirect detection of dark matter with neutrinos, Zenodo (202)0.
- [121] XENON collaboration, Light dark matter search with ionization signals in XENON1T, Phys. Rev. Lett. 123 (2019) 251801 [arXiv:1907.11485] [INSPIRE].
- [122] PANDAX collaboration, Dark matter search results from the commissioning run of PandaX-II, Phys. Rev. D 93 (2016) 122009 [arXiv:1602.06563] [INSPIRE].
- [123] LUX collaboration, Results from a search for dark matter in the complete LUX exposure, Phys. Rev. Lett. 118 (2017) 021303 [arXiv:1608.07648] [INSPIRE].
- [124] PICO collaboration, Dark matter search results from the complete exposure of the PICO-60 C_3F_8 bubble chamber, Phys. Rev. D 100 (2019) 022001 [arXiv:1902.04031] [INSPIRE].
- [125] G. Jungman, M. Kamionkowski and K. Griest, Supersymmetric dark matter, Phys. Rept. 267 (1996) 195 [hep-ph/9506380] [INSPIRE].
- [126] H.S Friese, Virgil's Aeneid. Books I–VI, with introduction, notes, and vocabulary, American book co., U.S.A. (1902).
- [127] C.A. Argüelles, J. Salvado and C.N. Weaver, ν-SQuIDS, https://github.com/Arguelles/nuSQuIDS (2015).
- [128] C.A. Argüelles, J. Salvado and C.N. Weaver, A Simple Quantum Integro-Differential Solver (SQuIDS), Comput. Phys. Commun. 255 (2020) 107405.
- [129] P. Ciafaloni, D. Comelli, A. Riotto, F. Sala, A. Strumia and A. Urbano, Weak corrections are relevant for dark matter indirect detection, JCAP 03 (2011) 019 [arXiv:1009.0224] [INSPIRE].
- [130] M. Pospelov, A. Ritz and M.B. Voloshin, Secluded WIMP dark matter, Phys. Lett. B 662 (2008) 53 [arXiv:0711.4866] [INSPIRE].
- [131] M. Cirelli et al., PPPC 4 DM ID: a Poor Particle Physicist Cookbook for dark matter indirect detection, JCAP 03 (2011) 051 [Erratum ibid. 10 (2012) E01] [arXiv:1012.4515] [INSPIRE].
- [132] N. Bozorgnia and G. Bertone, Implications of hydrodynamical simulations for the interpretation of direct dark matter searches, Int. J. Mod. Phys. A 32 (2017) 1730016 [arXiv:1705.05853] [INSPIRE].
- [133] Y. Ascasibar, P. Jean, C. Boehm and J. Knoedlseder, Constraints on dark matter and the shape of the Milky Way dark halo from the 511-keV line, Mon. Not. Roy. Astron. Soc. 368 (2006) 1695 [astro-ph/0507142] [INSPIRE].
- [134] B. Robertson and A. Zentner, Dark matter annihilation rates with velocity-dependent annihilation cross sections, Phys. Rev. D 79 (2009) 083525 [arXiv:0902.0362] [INSPIRE].
- [135] F. Ferrer and D.R. Hunter, The impact of the phase-space density on the indirect detection of dark matter, JCAP **09** (2013) 005 [arXiv:1306.6586] [INSPIRE].

- [136] S. Campbell and B. Dutta, Effects of P-wave annihilation on the angular power spectrum of extragalactic gamma-rays from dark matter annihilation, Phys. Rev. D 84 (2011) 075004 [arXiv:1106.4621] [INSPIRE].
- [137] R. Diamanti, L. Lopez-Honorez, O. Mena, S. Palomares-Ruiz and A.C. Vincent, Constraining dark matter late-time energy injection: decays and P-wave annihilations, JCAP 02 (2014) 017 [arXiv:1308.2578] [INSPIRE].
- [138] K.K. Boddy, J. Kumar, L.E. Strigari and M.-Y. Wang, Sommerfeld-Enhanced j-factors for dwarf spheroidal galaxies, Phys. Rev. D 95 (2017) 123008 [arXiv:1702.00408] [INSPIRE].
- [139] B.-Q. Lu, Y.-L. Wu, W.-H. Zhang and Y.-F. Zhou, Constraints on the Sommerfeld-enhanced dark matter annihilation from the gamma rays of subhalos and dwarf galaxies, JCAP 04 (2018) 035 [arXiv:1711.00749] [INSPIRE].
- [140] S. Bergström et al., *J-factors for self-interacting dark matter in 20 dwarf spheroidal galaxies*, *Phys. Rev. D* **98** (2018) 043017 [arXiv:1712.03188] [INSPIRE].
- [141] M. Petac, P. Ullio and M. Valli, On velocity-dependent dark matter annihilations in dwarf satellites, JCAP 12 (2018) 039 [arXiv:1804.05052] [INSPIRE].
- [142] K.K. Boddy, J. Kumar and L.E. Strigari, Effective J-factor of the Galactic Center for velocity-dependent dark matter annihilation, Phys. Rev. D 98 (2018) 063012 [arXiv:1805.08379] [INSPIRE].
- [143] K.K. Boddy, J. Kumar, A.B. Pace, J. Runburg and L.E. Strigari, Effective J-factors for Milky Way dwarf spheroidal galaxies with velocity-dependent annihilation, Phys. Rev. D 102 (2020) 023029 [arXiv:1909.13197] [INSPIRE].
- [144] C.A. Argüelles, A. Diaz, A. Kheirandish, A. Olivares-Del-Campo, I. Safa and A.C. Vincent, Dark matter annihilation to neutrinos: an updated, consistent & compelling compendium of constraints, arXiv:1912.09486 [INSPIRE].
- [145] A. Gould, WIMP distribution in and evaporation from the Sun, Astrophys. J. **321** (1987) 560 [INSPIRE].
- [146] R. Catena and A. Widmark, WIMP capture by the Sun in the effective theory of dark matter self-interactions, JCAP 12 (2016) 016 [arXiv:1609.04825] [INSPIRE].
- [147] R. Catena, WIMP capture and annihilation in the Earth in effective theories, JCAP 01 (2017) 059 [arXiv:1609.08967] [INSPIRE].
- [148] A. Gould, Cosmological density of WIMPs from solar and terrestrial annihilations, Astrophys. J. 388 (1992) 338 [INSPIRE].
- [149] N. Vinyoles et al., A new generation of standard solar models, Astrophys. J. 835 (2017) 202 [arXiv:1611.09867] [INSPIRE].
- [150] F. Halzen and D. Hooper, The indirect search for dark matter with IceCube, New J. Phys. 11 (2009) 105019 [arXiv:0910.4513] [INSPIRE].
- [151] GAMBIT collaboration, Global analyses of Higgs portal singlet dark matter models using GAMBIT, Eur. Phys. J. C 79 (2019) 38 [arXiv:1808.10465] [INSPIRE].
- [152] A. Vincent, N. Kozar and P. Scott, aaronvincent/captagen, Zenodo (2020).
- [153] K. Choi, C. Rott and Y. Itow, Impact of the dark matter velocity distribution on capture rates in the Sun, JCAP **05** (2014) 049 [arXiv:1312.0273] [INSPIRE].
- [154] ICECUBE, PICO collaboration, Velocity Independent Constraints on Spin-Dependent DM-Nucleon Interactions from IceCube and PICO, Eur. Phys. J. C 80 (2020) 819 [arXiv:1907.12509] [INSPIRE].
- [155] J. Edsjo, Aspects of neutrino detection of neutralino dark matter, other thesis, 4, 1997 [hep-ph/9704384] [INSPIRE].

- [156] S. Ritz and D. Seckel, Detailed neutrino spectra from cold dark matter annihilations in the Sun, Nucl. Phys. B **304** (1988) 877 [INSPIRE].
- [157] J.D. Jackson, *Classical electrodynamics*, 3rd edition, Wiley, New York U.S.A. (1999), see chapter 13 problem 13.6(b).
- [158] J.H. Koehne et al., *PROPOSAL*: a tool for propagation of charged leptons, *Comput. Phys. Commun.* **184** (2013) 2070 [INSPIRE].
- [159] L.I. Ponomarev, Molecular structure effects on atomic and nuclear capture of mesons, Ann. Rev. Nucl. Part. Sci. 23 (1973) 395 [INSPIRE].
- [160] M.L. Good, Relation between scattering and absorption in the Pais-Piccioni phenomenon, Phys. Rev. 106 (1957) 591 [INSPIRE].
- [161] C. Garcia-Cely and J. Heeck, *Indirect searches of dark matter via polynomial spectral features*, JCAP 08 (2016) 023 [arXiv:1605.08049] [INSPIRE].
- [162] C. Niblaeus, J.M. Cornell and J. Edsjö, Effect of polarisation and choice of event generator on spectra from dark matter annihilations, JCAP 10 (2019) 079 [arXiv:1907.02488] [INSPIRE].
- [163] R. Gandhi, C. Quigg, M.H. Reno and I. Sarcevic, Neutrino interactions at ultrahigh-energies, Phys. Rev. D 58 (1998) 093009 [hep-ph/9807264] [INSPIRE].
- [164] J.A. Formaggio and G.P. Zeller, From eV to EeV: neutrino cross sections across energy scales, Rev. Mod. Phys. 84 (2012) 1307 [arXiv:1305.7513] [INSPIRE].
- [165] S. Kretzer and M.H. Reno, Tau neutrino deep inelastic charged current interactions, Phys. Rev. D 66 (2002) 113007 [hep-ph/0208187] [INSPIRE].
- [166] E.A. Paschos and J.Y. Yu, Neutrino interactions in oscillation experiments, Phys. Rev. D 65 (2002) 033002 [hep-ph/0107261] [INSPIRE].
- [167] K. Hagiwara, K. Mawatari and H. Yokoya, Tau polarization in tau neutrino nucleon scattering, Nucl. Phys. B 668 (2003) 364 [Erratum ibid. 701 (2004) 405] [hep-ph/0305324] [INSPIRE].
- [168] J. Conrad, A. de Gouvêa, S. Shalgar and J. Spitz, Atmospheric tau neutrinos in a multi-kiloton Liquid Argon Detector, Phys. Rev. D 82 (2010) 093012 [arXiv:1008.2984] [INSPIRE].
- [169] F. Halzen and D. Saltzberg, Tau-neutrino appearance with a 1000 megaparsec baseline, Phys. Rev. Lett. 81 (1998) 4305 [hep-ph/9804354] [INSPIRE].
- [170] C. Giunti and C.W. Kim, Fundamentals of neutrino physics and astrophysics, Oxford University Press, Oxford U.K. (2007).
- [171] T2K collaboration, Constraint on the matter-antimatter symmetry-violating phase in neutrino oscillations, Nature **580** (2020) 339 [Erratum ibid. **583** (2020) E16] [arXiv:1910.03887] [INSPIRE].
- [172] I. Esteban, M.C. Gonzalez-Garcia, A. Hernandez-Cabezudo, M. Maltoni and T. Schwetz, NuFIT, version 4.1 (2019), www.nu-fit.org.
- [173] J. Edsjö, Calculation of neutrino cross sections and the nusigma neutrino-nucleon scattering Monte Carlo, unpublished (2007).
- [174] A.M. Dziewonski and D.L. Anderson, Preliminary reference earth model, Phys. Earth Planet. Int. 25 (1981) 297.
- [175] M. Pospelov and A. Ritz, Astrophysical Signatures of Secluded Dark Matter, Phys. Lett. B 671 (2009) 391 [arXiv:0810.1502] [INSPIRE].
- [176] P. Meade, S. Nussinov, M. Papucci and T. Volansky, Searches for Long Lived Neutral Particles, JHEP 06 (2010) 029 [arXiv:0910.4160] [INSPIRE].

- [177] P. Schuster, N. Toro and I. Yavin, Terrestrial and solar limits on long-lived particles in a dark sector, Phys. Rev. D 81 (2010) 016002 [arXiv:0910.1602] [INSPIRE].
- [178] M. Ardid, I. Felis, A. Herrero and J.A. Martínez-Mora, Constraining secluded dark matter models with the public data from the 79-string IceCube search for dark matter in the Sun, JCAP 04 (2017) 010 [arXiv:1701.08863] [INSPIRE].
- [179] R.K. Leane, K.C.Y. Ng and J.F. Beacom, Powerful solar signatures of long-lived dark mediators, Phys. Rev. D 95 (2017) 123016 [arXiv:1703.04629] [INSPIRE].
- [180] I. Cholis, D.P. Finkbeiner, L. Goodenough and N. Weiner, *The PAMELA positron excess from annihilations into a light boson*, *JCAP* **12** (2009) 007 [arXiv:0810.5344] [INSPIRE].
- [181] AMS collaboration, First Result from the Alpha Magnetic Spectrometer on the International Space Station: Precision Measurement of the Positron Fraction in Primary Cosmic Rays of 0.5–350 GeV, Phys. Rev. Lett. 110 (2013) 141102 [INSPIRE].
- [182] C. Niblaeus, A. Beniwal and J. Edsjo, Neutrinos and gamma rays from long-lived mediator decays in the Sun, JCAP 11 (2019) 011 [arXiv:1903.11363] [INSPIRE].
- [183] S. Amoroso, S. Caron, A. Jueid, R. Ruiz de Austri and P. Skands, Estimating QCD uncertainties in Monte Carlo event generators for gamma-ray dark matter searches, JCAP 05 (2019) 007 [arXiv:1812.07424] [INSPIRE].
- [184] P. Gondolo, J. Edsjo, P. Ullio, L. Bergstrom, M. Schelke and E.A. Baltz, *DarkSUSY:* computing supersymmetric dark matter properties numerically, *JCAP* **07** (2004) 008 [astro-ph/0406204] [INSPIRE].
- [185] T. Bringmann, J. Edsjö, P. Gondolo, P. Ullio and L. Bergström, *DarkSUSY 6: an advanced tool to compute dark matter properties numerically*, *JCAP* **07** (2018) 033 [arXiv:1802.03399] [INSPIRE].
- [186] ICECUBE collaboration, Search for neutrinos from dark matter self-annihilations in the center of the Milky Way with 3 years of IceCube/DeepCore, Eur. Phys. J. C 77 (2017) 627 [arXiv:1705.08103] [INSPIRE].
- [187] ANTARES, ICECUBE collaboration, Combined search for neutrinos from dark matter self-annihilation in the Galactic Centre with ANTARES and IceCube, arXiv:2003.06614 [INSPIRE].
- [188] A. Albert et al., Results from the search for dark matter in the Milky Way with 9 years of data of the ANTARES neutrino telescope, Phys. Lett. B 769 (2017) 249 [Erratum ibid. 796 (2019) 253] [arXiv:1612.04595] [INSPIRE].
- [189] A. Cooper-Sarkar, P. Mertsch and S. Sarkar, The high energy neutrino cross-section in the Standard Model and its uncertainty, JHEP 08 (2011) 042 [arXiv:1106.3723] [INSPIRE].
- [190] C. Delaunay, P.J. Fox and G. Perez, *Probing dark matter dynamics via Earthborn neutrinos at IceCube*, *JHEP* **05** (2009) 099 [arXiv:0812.3331] [INSPIRE].
- [191] J.L. Feng, J. Smolinsky and P. Tanedo, Detecting dark matter through dark photons from the Sun: Charged particle signatures, Phys. Rev. D 93 (2016) 115036 [Erratum ibid. 96 (2017) 099903] [arXiv:1602.01465] [INSPIRE].